J. Fluid Mech. (1986), *vol.* 166, *pp.* 503–530
Printed in Great Britain

Free convection in an undulating saturated porous layer: resonant wavelength excitation

By D. A. S. REES AND D. S. RILEY
School of Mathematics, University Walk, Bristol BS8 1TW

(Received 16 July 1985 and in revised form 8 January 1986)

Thermal convection in a saturated porous medium contained between two undulating fixed boundaries of mean horizontal disposition is considered when the layer is heated from below. In an analytic study, the amplitudes of the two-dimensional undulations are assumed to be small compared with the mean depth, and the wavelength is taken to be close to the critical wavelength for the onset of Lapwood convection. For values of the mean Darcy–Rayleigh number Ra below the Lapwood critical value Ra_c an analytical formula is found for the mean Nusselt number. As $Ra \to Ra_c$, convection driven by baroclinic effects induced by boundary variations is greatly amplified by convective instabilities. The natures of the resultant bifurcations are examined when the configuration is varicose and also non-varicose. Consideration is given to both longitudinal and transverse modes and to the effects of detuning. The effects of finite amplitude and larger Rayleigh number are examined, for the varicose configuration, in a numerical study of two-dimensional convection. Periodic solutions are found and the existence of the flows delimited in the parameter space of Ra and the boundary amplitude a.

1. Introduction

The phenomenon of buoyancy-induced flow and heat transfer through a saturated porous medium has attracted considerable attention over the last twenty years. This interest in thermal convection through porous media has been stimulated in two ways. First, there are diverse applications in, for example, chemical engineering, geothermal energy and hydrocarbon reservoir modelling, thermal-insulation engineering, and such geophysical phenomena as frost heave. Secondly, the problem provides a relatively simple test-bed for the development of analytical and numerical techniques for studying thermal instability, bifurcation and transition to turbulence in a Newtonian fluid. Moreover, porous media also provide a convenient means of studying experimentally such phenomena as cell-pattern selection and hysteresis.

The present study is aimed at examining the geometrical effects of two-dimensional spatially periodic boundary variations upon the Lapwood problem (i.e. an unstably stratified Boussinesq fluid saturating a porous medium bounded between two smooth, horizontal boundaries of infinite extent with constant, but unequal temperatures).The motivation for initiating this study was geophysical, namely the application to convection within a saturated porous medium such as a folded rock stratum. In the context of geophysical applications, the assumption of isothermal boundaries, i.e. perfectly conducting boundaries, must be questionable. Indeed recent work by Riahi (1983) does address itself to the problem of porous layers with finite conducting boundaries. In this paper, however, we choose to simplify the problem by confining

our attention to the perfectly conducting case. Nevertheless, it is not our intention to consider a particular application of our results.

The onset of convection in a plane horizontal porous layer was first investigated using linear stability theory by Lapwood (1948). Subsequently, Palm, Weber & Kvernvold (1972) employed weakly nonlinear theory to investigate moderately supercritical flow, while Straus (1974) used spectral methods to further extend the results. Palm *et al.* reported, and the results of Straus confirmed, that two-dimensional motion is the only stable mode for moderately supercritical Rayleigh numbers in the Lapwood problem. It is natural therefore that we concentrate on two-dimensional modes – this is the spirit in which most thermal-convection studies are undertaken, especially in problems involving imperfections.

Other literature directly related to this problem is generally concerned with convection of Newtonian fluids in horizontal slots, rather than saturated porous media. Watson & Poots (1971) seem to be the first to have studied the effect of boundary variations on free convection. Their study of convection in a *vertical* slot was motivated by an interest in optimizing the heat transfer from wavy-walled boilers. Vozovoi & Nepomnyaschii (1974), Tavantzis, Reiss & Matkowsky (1978), and Kelly & Pal (1976, 1978), Pal & Kelly (1978, 1979) have variously described the effects of periodic, small-amplitude boundary non-uniformities in either the temperature or location. On the other hand Eagles (1980) and Walton (1982*a*, *b*) have considered similar non-uniformities which are also slow, i.e. occur over a long scale. Of all these references, Kelly & Pal (1978) is the most pertinent.

In our analytical work, the amplitudes of the boundary variations are taken to be $O(\delta)$, where $\delta \ll 1$, and expansions are made in terms of δ. The wavenumber of the periodic variations of both boundaries is assumed to lie close or equal to the critical wavenumber ($k_c = \frac{1}{2}\pi$) characteristic of the classical Lapwood problem and so, as in Kelly & Pal (1978), the problem generally involves resonant wavelength excitation.

In the Lapwood problem no steady convection is possible until the Rayleigh number Ra is greater than the critical value $Ra_c = \pi^2$ for linear stability. When there are boundary variations, however, fluid motion always occurs, whatever the non-zero value of the Rayleigh number, due to the baroclinic effect. In §3 the 'quasi-conduction' regime, wherein $Ra \ll Ra_c$ and the convection has amplitude $O(\delta)$, is analysed and asymptotic expansions found for the stream function, the temperature and hence the Nusselt number. For a configuration which is not exactly varicose, these expansions become singular as $Ra \to Ra_c$ – and a rescaling is necessary which balances the growing amplitude of $O(\delta/(Ra - Ra_c))$ with the amplitude of the motion due to the classical Lapwood convective instability of $O((Ra - Ra_c)^{\frac{1}{2}})$; this is considered in §4. In §4.1 two-dimensional flow is studied and a governing cubic equation found for the amplitude of convection. This equation yields three supercritical states but only the mode connected to the subcritical state is found to be stable. In §4.2 a three-dimensional formulation is introduced and a study made of the interaction between longitudinal and transverse rolls, together with the effect of a small detuning of the boundary wavenumber from k_c. It is found that there is no purely transverse mode, but there are three situations depending on the detuning, in which purely longitudinal and mixed modes coexist.

If the configuration is varicose, the expansions of §3 remain regular, but there is a supercritical bifurcation near $Ra = Ra_c$; this is analysed in §5. In §5.1 two-dimensional motion is considered and the shift in the critical Rayleigh number due to boundary non-uniformities calculated. It is found that two modes bifurcate near $Ra = Ra_c$; one, termed type I, stable in the infinite layer and the other, termed type

II, stable, for example, in an infinite cylinder. In §5.2 the interactions between longitudinal and transverse rolls with amplitudes $O(\delta)$ are studied. In this case, a stable purely transverse mode is first to bifurcate. There is also a purely longitudinal mode which is unstable until it suffers a secondary bifurcation to an unstable mixed mode.

Finally in §6, a numerical study is presented of the varicose case for finite boundary amplitudes and for Rayleigh numbers up to 40. It is found that there exist two distinct modes of two-dimensional flow, one of which is fluctuating, the other being steady and consisting of either two or four cells.

2. Formulation of the problem

We consider an undulating porous layer, of mean vertical depth $2d$ and of infinite horizontal extent, saturated with fluid. The mean disposition of the layer is horizontal and we use a Cartesian coordinate system with $\hat{z}$ vertical and $\hat{x}$ in the horizontal direction of the boundary variation. The upper and lower boundaries are taken to be impermeable and isothermal at temperatures T_u and $T_l (T_u < T_l)$ respectively, which yield a natural characteristic temperature scale $\Delta T = \frac{1}{2}(T_l - T_u)$. Other variables are non-dimensionalized with respect to length, velocity, pressure and time scales given by d, $\lambda_m/(\rho_f c_f d)$, $\nu\lambda_m/(Kc_f)$ and $\rho_m c_m d^2/\lambda_m$ respectively. Here λ_m, ρ_m, c_m are the thermal conductivity, density and specific heat of the saturated porous medium; ν and c_f are the kinematic viscosity and specific heat of the saturating fluid, which has a reference density ρ_f. Then, on assuming that the Prandtl–Darcy number is large and invoking the Boussinesq approximation, the non-dimensionalized Darcy–Boussinesq equations become:

$$\boldsymbol{q} = -\nabla p + Ra\,\theta\hat{\boldsymbol{z}}, \tag{2.1}$$

$$\nabla\cdot\boldsymbol{q} = 0, \tag{2.2}$$

$$\frac{\partial\theta}{\partial t} + (\boldsymbol{q}\cdot\nabla)\,\theta = \nabla^2\theta, \tag{2.3}$$

where $\boldsymbol{q}$ is the Darcy velocity vector, p the pressure and θ is the temperature. $Ra = \beta g K \Delta T d \rho_f c_f/\nu\lambda_m$ is the Rayleigh number with β the coefficient of cubical expansion of the saturating fluid, K the permeability and g the acceleration due to gravity.

The boundary conditions needed to complete the specification of the problem are

$$\boldsymbol{q}\cdot\boldsymbol{n} = 0, \quad \theta = -1 \quad \text{(upper boundary)}, \tag{2.4}$$

$$\boldsymbol{q}\cdot\boldsymbol{n} = 0, \quad \theta = +1 \quad \text{(lower boundary)}, \tag{2.5}$$

where $\boldsymbol{n}$ denotes the normal to the boundary. In addition we assume that there is zero net horizontal volumetric flux.

3. Quasi-conduction regime

It is easily shown that small-amplitude steady solutions yield the critical Rayleigh number Ra_c above which non-decaying solutions exist for the full non-linear Lapwood problem (Beck 1972). Thus by continuity, we expect that for Ra sufficiently below Ra_c the flow between small-amplitude wavy boundaries is unique, stable and, since

the flow arises owing to the non-uniformities of the boundaries, two-dimensional. Thus on introducing a stream function ψ such that $\boldsymbol{q} = \operatorname{curl}(\psi\hat{\boldsymbol{y}})$, we have

$$\nabla^2\psi = Ra\,\theta_x, \tag{3.1}$$

$$\nabla^2\theta = J(\psi, \theta)+\theta_t, \tag{3.2}$$

with

$$\left.\begin{aligned}\psi &= 0\\ \theta &= -1\end{aligned}\right\} \quad \text{on } z = 1+\delta g_{\mathrm{u}}(x), \tag{3.3}$$

$$\left.\begin{aligned}\psi &= 0\\ \theta &= 1\end{aligned}\right\} \quad \text{on } z = -1-\delta g_{\mathrm{l}}(x). \tag{3.4}$$

Here ∇^2 denotes the two-dimensional Laplacian in x and z,

$$J(\psi, \theta) = \frac{\partial\psi}{\partial x}\frac{\partial\theta}{\partial z}-\frac{\partial\psi}{\partial z}\frac{\partial\theta}{\partial x} \tag{3.5}$$

and $g_{\mathrm{u}}(x)$, $g_{\mathrm{l}}(x)$ denote the shape functions of the upper and lower boundaries respectively. We take

$$g_{\mathrm{u}}(x) = a_{\mathrm{u}}\cos(kx-\beta), \quad g_{\mathrm{l}}(x) = a_{\mathrm{l}}\cos(kx+\beta), \tag{3.6}$$

where 2β is the phase difference between the two wavy boundaries, and a_{u}, a_{l} are amplitude measures for the respective boundaries.

It is convenient at this stage to introduce new independent variables ξ and η such that

$$\xi = x, \quad \eta = \frac{2z+\delta[g_{\mathrm{l}}(x)-g_{\mathrm{u}}(x)]}{2+\delta[g_{\mathrm{l}}(x)+g_{\mathrm{u}}(x)]}, \tag{3.7}$$

which transform the upper and lower boundaries to $\eta = \pm 1$.

Equations (3.1), (3.2) become

$$\mathrm{L}_1\psi = Ra\,\mathrm{L}_2\theta, \tag{3.8}$$

$$\mathrm{L}_1\theta = 2s_1 J(\psi, \theta)+s_1^2\frac{\partial\theta}{\partial t}, \tag{3.9}$$

where

$$J(\psi, \theta) = \frac{\partial\psi}{\partial\xi}\frac{\partial\theta}{\partial\eta}-\frac{\partial\psi}{\partial\eta}\frac{\partial\theta}{\partial\xi},$$

$$\mathrm{L}_1 \equiv s_1^2\frac{\partial^2}{\partial\xi^2}+2\delta s_1 s_2\frac{\partial^2}{\partial\eta\,\partial\xi}+[4+\delta^2 s_2^2]\frac{\partial^2}{\partial\eta^2}+[\delta s_1\{(1-\eta)g_{\mathrm{l}}''-(1+\eta)g_{\mathrm{u}}''\}-2\delta^2 s_2\{g_{\mathrm{l}}'+g_{\mathrm{u}}'\}]\frac{\partial}{\partial\eta},$$

$$\mathrm{L}_2 \equiv s_1^2\frac{\partial}{\partial\xi}+\delta s_1 s_2\frac{\partial}{\partial\eta},$$

with

$$s_1 = 2+\delta(g_{\mathrm{l}}+g_{\mathrm{u}}),$$

$$s_2 = (1-\eta)g_{\mathrm{l}}'-(1+\eta)g_{\mathrm{u}}'.$$

On assuming that $\delta \ll 1$ and that Ra is sufficiently below Ra_{c} (to be made more precise later) we look for steady-state solutions and expand:

$$\psi(\xi, \eta) = \delta\psi_1(\xi, \eta)+\delta^2\psi_2(\xi, \eta)+\ldots, \tag{3.10a}$$

$$\theta(\xi, \eta) = -\eta+\delta\theta_1(\xi, \eta)+\delta^2\theta_2(\xi, \eta)+\ldots. \tag{3.10b}$$

The $O(1)$ terms constitute the pure-conduction solution, whilst the $O(\delta)$ terms satisfy

$$\nabla^2\psi_1 - Ra\,\theta_{1\xi} = \tfrac{1}{2}Ra\,k[(1-\eta)\,a_1\sin(k\xi+\beta)-(1+\eta)\,a_u\sin(k\xi-\beta)], \quad (3.11a)$$

$$\nabla^2\theta_1 + \psi_{1\xi} = -\tfrac{1}{2}k^2[(1-\eta)\,a_1\cos(k\xi+\beta)+(1+\eta)\,a_u\cos(k\xi-\beta)], \quad (3.11b)$$

with $\psi_1 = \theta_1 = 0$ on $\eta = \pm 1$. These equations are readily solved:

$$\psi_1 = a_1 f_1(\eta)\sin(k\xi+\beta)+a_u f_2(\eta)\sin(k\xi-\beta), \quad (3.12a)$$

$$\theta_1 = a_1 g_1(\eta)\cos(k\xi+\beta)+a_u g_2(\eta)\cos(k\xi-\beta), \quad (3.12b)$$

where

$$f_1(\eta) = \tfrac{1}{4}Ra^{\frac{1}{2}}\left[\frac{\sinh(\chi\eta)}{\sinh(\chi)}-\frac{\cosh(\chi\eta)}{\cosh(\chi)}-\frac{\sinh(\gamma\eta)}{\sinh(\gamma)}+\frac{\cosh(\gamma\eta)}{\cosh(\gamma)}\right], \quad (3.13a)$$

$$f_2(\eta) = \tfrac{1}{4}Ra^{\frac{1}{2}}\left[\frac{\sinh(\chi\eta)}{\sinh(\chi)}+\frac{\cosh(\chi\eta)}{\cosh(\chi)}-\frac{\sinh(\gamma\eta)}{\sinh(\gamma)}-\frac{\cosh(\gamma\eta)}{\cosh(\gamma)}\right], \quad (3.13b)$$

$$g_1(\eta) = \frac{1}{4}\left[\frac{\sinh(\chi\eta)}{\sinh(\chi)}-\frac{\cosh(\chi\eta)}{\cosh(\chi)}+\frac{\sinh(\gamma\eta)}{\sinh(\gamma)}-\frac{\cosh(\gamma\eta)}{\cosh(\gamma)}+2-2\eta\right], \quad (3.13c)$$

$$g_2(\eta) = \frac{1}{4}\left[\frac{\sinh(\chi\eta)}{\sinh(\chi)}+\frac{\cosh(\chi\eta)}{\cosh(\chi)}+\frac{\sinh(\gamma\eta)}{\sinh(\gamma)}+\frac{\cosh(\gamma\eta)}{\cosh(\gamma)}-2-2\eta\right]. \quad (3.13d)$$

Here χ, which may be real or imaginary, and γ are given by

$$\gamma^2 = k^2 + k\,Ra^{\frac{1}{2}}, \quad \chi^2 = k^2 - k\,Ra^{\frac{1}{2}}, \quad (3.14a, b)$$

with $\chi = \gamma = k$ when $Ra = 0$.

These solutions are valid for all wall wavenumbers k, but in general become singular in the limit $\cosh\chi \to 0$. Using (3.14), we see that for a given wavenumber k this behaviour first occurs as $Ra \to \mathscr{R}_c$, where

$$\mathscr{R}_c = \frac{(k^2+\frac{1}{4}\pi^2)^2}{k^2}, \quad (3.15)$$

which is precisely the expression for the neutral stability curve in the Lapwood problem. This type of behaviour was first noted by Watson & Poots (1971) and again later by Kelly & Pal (1976). Thus as $Ra \to Ra_c$ with $k \sim k_c$, (3.10*a*, *b*) break down and new expansions must be determined. For the Bénard problem, this resonant case was simultaneously attacked by Tavantzis, Reiss & Matkowsky (1978) and Kelly & Pal (1976, 1978).

When the layer is varicose, that is $a_u = a_1 = a$, say, and $\beta = 0$ (see figure 1*a*), the first-order solution reduces to

$$\psi_1 = \tfrac{1}{2}a\,Ra^{\frac{1}{2}}\left[\frac{\sinh(\chi\eta)}{\sinh(\chi)}-\frac{\sinh(\gamma\eta)}{\sinh(\gamma)}\right]\sin(k\xi), \quad (3.16a)$$

$$\theta_1 = \tfrac{1}{2}a\left[\frac{\sinh(\chi\eta)}{\sinh(\chi)}+\frac{\sinh(\gamma\eta)}{\sinh(\gamma)}-2\eta\right]\cos(k\xi), \quad (3.16b)$$

which remains bounded near the neutral stability curve. This was noted by Kelly & Pal (1978) but pursued no further; discussion of this special case is left until §5.

In figure 1, we display the $O(\delta)$ streamlines for $Ra = 5$, $a_u = a_1$, and various wall phases β. For the varicose configuration, $\beta = 0$, the flow consists of a set of four counter-rotating cells per wall wavelength, as expected from symmetry considerations. As shown, this pattern is quickly distorted by small deviations of β away from zero,

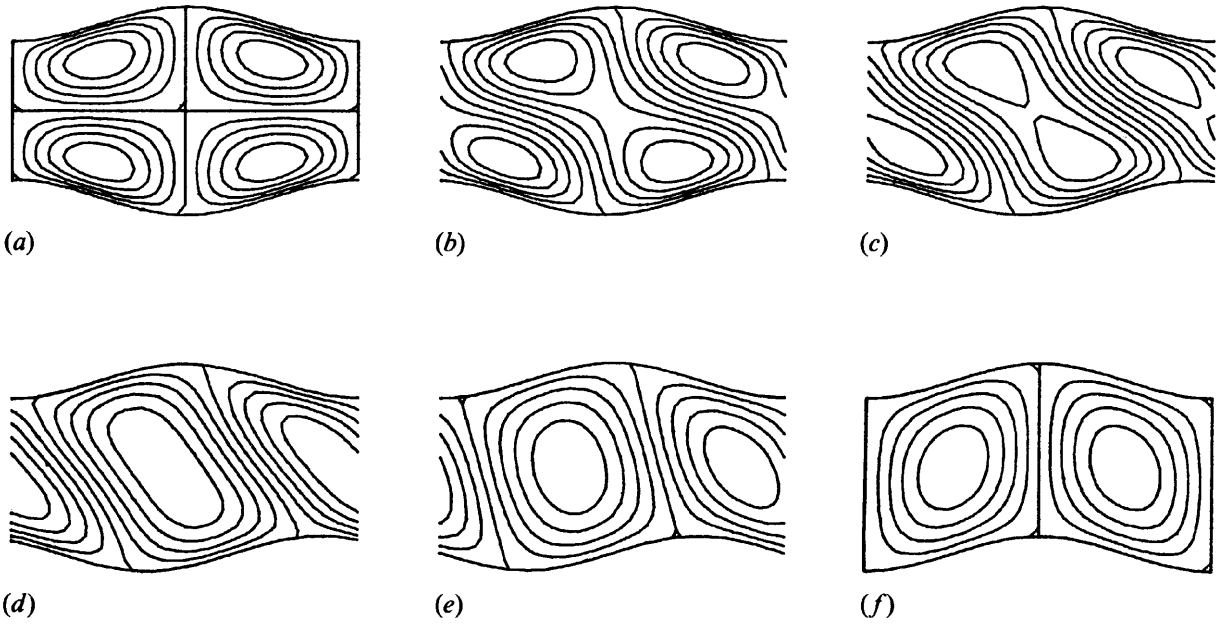

FIGURE 1. The $O(\delta)$ streamlines as calculated from equation (3.12a) for $Ra = 5$, $a_u = a_l$, and wall phases (a) 0°, (b) 5°, (c) 10°, (d) 20°, (e) 45°, (f) 90°.

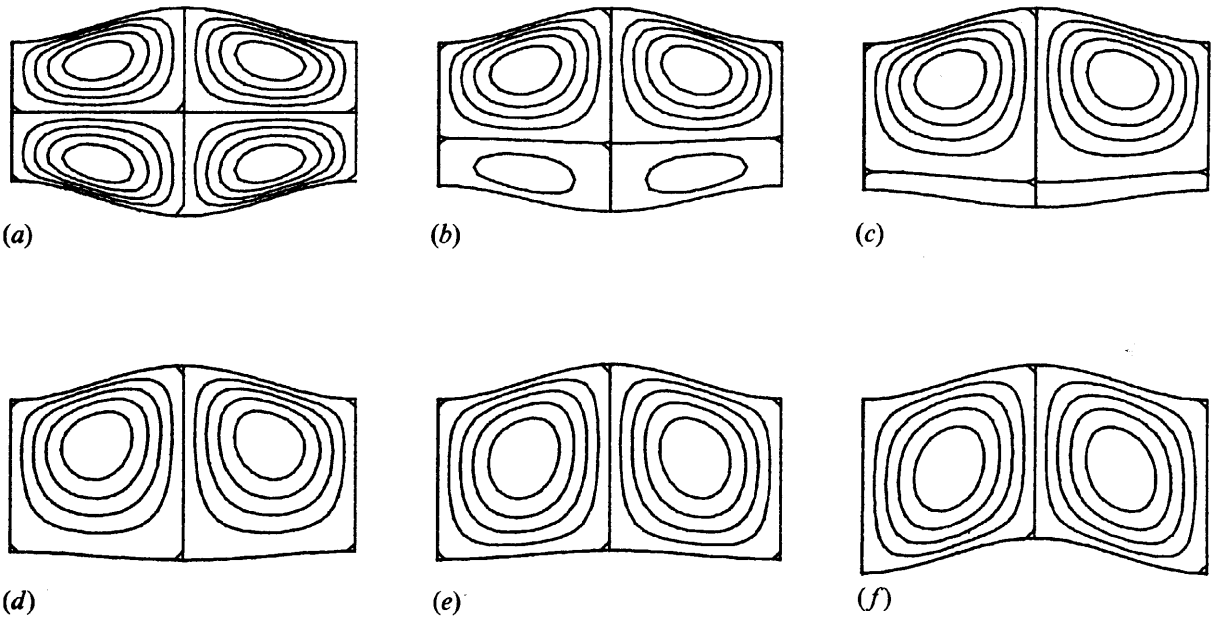

FIGURE 2. The $O(\delta)$ streamlines as calculated from equation (3.12a) for $Ra = 5$, $\beta = 0$ and wall amplitudes (a) $a_l = a_u$, (b) $a_l = 0.75a_u$, (c) $a_l = 0.5a_u$, (d) $a_l = 0.25a_u$, (e) $a_l = -0.25a_u$, (f) $a_l = -a_u$.

with pairs of cells coalescing as $|\beta|$ increases. The sense of the flow is always such that it is up the hotter, lower boundary and down the cooler, upper boundary.

Again from symmetry considerations, we expect a symmetrical two-cell pattern when $\beta = 0$ and $a_u = -a_l$, i.e. for the sinuous case (see figure 1f). This is shown in figure 2 along with the effect of varying a_l whilst holding a_u fixed with $\beta = 0$ and $Ra = 5$.

The boundary non-uniformities may induce distortions at $O(\delta^2)$ to the mean values (i.e. averages over one boundary wavelength) of horizontal flow and heat transfer. Omitting all algebraic details, it is found that the mean flow is non-zero, except if $\beta = 0$ or π, or if one of the boundaries is flat, i.e. a_u or $a_l = 0$. Of more importance, however, is the mean heat transfer. On using $\lambda_m d/\Delta T$ to non-dimensionalize the local

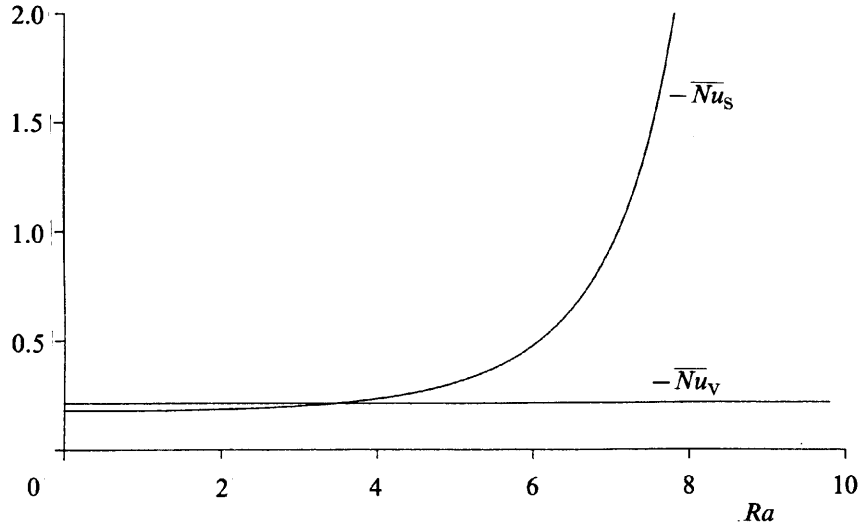

FIGURE 3. The second-order Nusselt numbers (from equation (3.18)) for $k = k_c$.

conductive heat transfer from the lower boundary, the mean Nusselt number $\overline{Nu}$ is given by (cf. Watson & Poots):

$$\overline{Nu} = \frac{k}{2\pi}\int_0^{2\pi/k}\left(\frac{1+[\delta g_1']^2}{1+\frac{1}{2}\delta[g_1+g_u]}\right)\left(\frac{\partial\theta}{\partial\eta}\right)_{\eta=-1} d\xi. \tag{3.17}$$

It is found that

$$\overline{Nu} = -1+\delta^2[(a_1^2+a_u^2+2a_1a_u\cos 2\beta)\,\overline{Nu}_V + (a_1^2+a_u^2-2a_1a_u\cos 2\beta)\,\overline{Nu}_S] + o(\delta^2), \tag{3.18a}$$

where

$$\overline{Nu}_V = \frac{kRa^{\frac{1}{2}}}{64}\left[\frac{\coth(\gamma)}{\gamma}-\frac{\coth(\chi)}{\chi}+\coth^2\chi-\coth^2\gamma\right]-\tfrac{1}{16}[\chi\coth\chi+\gamma\coth\gamma], \tag{3.18b}$$

$$\overline{Nu}_S = \frac{kRa^{\frac{1}{2}}}{64}\left[\frac{\tanh\gamma}{\gamma}-\frac{\tanh\chi}{\chi}+\tanh^2\chi-\tanh^2\gamma\right]-\tfrac{1}{16}[\chi\tanh\chi+\gamma\tanh\gamma]. \tag{3.18c}$$

Here the heat transfer has been conveniently factored into varicose ($a_1 = a_u$, $\beta = 0$) and sinuous ($a_1 = -a_u$, $\beta = 0$) contributions. $\overline{Nu}_V$ and $\overline{Nu}_S$ are plotted in figure 3 and we note that they are always negative. Thus, since the coefficients of $\overline{Nu}_V$ and $\overline{Nu}_S$ in (3.18*a*) are non-negative, we conclude that the induced convection enhances the boundary heat transfer.

4. The critical regime for the non-varicose configuration

4.1. *Two-dimensional*

We follow Kelly & Pal (1978) and consider flow in a non-varicose layer with $k = k_c$ and $Ra \sim Ra_c$. According to Palm *et al.* (1972), two-dimensional motion is the only stable mode for moderately supercritical Rayleigh numbers in ordinary Lapwood convection. It is feasible that this result carries over to the present case when the boundary non-uniformities are infinitesimally small. The orientation of the rolls, however, is not obvious. It is plausible that the rolls will be longitudinal (i.e. with generators in the y-direction) and we first investigate this case.

The scalings appropriate to this type of problem have been fully discussed by Tavantzis *et al.* (1978) using matched asymptotic expansions, and by Kelly & Pal using heuristic reasoning. We initially consider steady solutions and take

$$\psi = \delta^{\frac{1}{3}} \Psi_{\frac{1}{3}} + \delta^{\frac{2}{3}} \Psi_{\frac{2}{3}} + \delta \Psi_1 + \dots, \tag{4.1a}$$

$$\theta = -\eta + \delta^{\frac{1}{3}} \Theta_{\frac{1}{3}} + \delta^{\frac{2}{3}} \Theta_{\frac{2}{3}} + \delta \Theta_1 + \dots, \tag{4.1b}$$

and

$$Ra = Ra_c + \delta^{\frac{2}{3}} Ra_{\frac{2}{3}} + \dots. \tag{4.1c}$$

The problem at order $\delta^{\frac{1}{3}}$ and $\delta^{\frac{2}{3}}$ are equivalent to the first- and second-order problems considered by Palm *et al.* in their study of supercritical convection in a porous medium. Omitting the detailed analysis, we have

$$\Psi_{\frac{1}{3}} = -2k_c A \cos(k_c \xi + \alpha) \cos k_c \eta, \tag{4.2a}$$

$$\Theta_{\frac{1}{3}} = A \sin(k_c \xi + \alpha) \cos k_c \eta, \tag{4.2b}$$

$$\Psi_{\frac{2}{3}} \equiv 0, \quad \Theta_{\frac{2}{3}} = \tfrac{1}{4} A^2 k_c \sin 2k_c \eta, \tag{4.3a, b}$$

where the amplitude A and phase α are to be determined. The equations for Ψ_1 and Θ_1 are then

$$\nabla^2 \Psi_1 - Ra_c \Theta_{1\xi} = \tfrac{1}{2} Ra_c k_c [(1-\eta) a_l \sin(k_c \xi + \beta) - (1+\eta) a_u \sin(k_c \xi - \beta)] + k_c Ra_{\frac{2}{3}} A \cos(k_c \xi + \alpha) \cos k_c \eta, \tag{4.4a}$$

$$\nabla^2 \Theta_1 + \Psi_{1\xi} = -\tfrac{1}{2} k_c^2 [(1-\eta) a_l \cos(k_c \xi + \beta) - (1+\eta) a_u \cos(k_c \xi - \beta)] + \tfrac{1}{2} k_c^4 A^3 \sin(k_c \xi + \alpha) [\cos k_c \eta + \cos 3k_c \eta], \tag{4.4b}$$

which must be solved subject to the vanishing of Ψ_1 and Θ_1 on $\eta = \pm 1$. If (4.4*a*) is multiplied by $\Psi_{\frac{1}{3}}/Ra_c$, (4.4*b*) by $\Theta_{\frac{1}{3}}$ and the resulting equations added and integrated over a wavelength in the ξ-direction and between -1 and $+1$ in the η-direction, the following solvability condition results:

$$k_c^4 A^3 - Ra_{\frac{2}{3}} A - 2k_c c^3 = 0, \tag{4.5a}$$

where c is the real root of

$$c^3 = [a_u \sin(\alpha + \beta) - a_l \sin(\alpha - \beta)]. \tag{4.5b}$$

We interpret (4.5*a*) as defining A in terms of $Ra_{\frac{2}{3}}$. As shown in figure 4, for $Ra_{\frac{2}{3}} > 3k_c^2 c^2$ there are three possible solutions to (4.5*a*). As $Ra_{\frac{2}{3}} \to \infty$, $A/c \sim \pm [Ra_{\frac{2}{3}}/(k_c^4 c^2)]^{\frac{1}{2}}$ on the upper and lower branches respectively, whilst $A/c \sim -2k_c^2 c^2/Ra_{\frac{2}{3}}$ on the middle branch.

We now turn to the questions of the preferred convective phase α and the relative stability of the three supercritical solutions. In order to address these questions we must allow for a slow time dependence in the amplitude A and phase α. Thus we introduce a slow timescale $\tau = \delta^{\frac{2}{3}} t$ into (3.9). The existence of solutions to the $O(\delta)$ equations requires that

$$\frac{dA}{d\tau} = -\tfrac{1}{2} \{k_c^4 A^3 - A\, Ra_{\frac{2}{3}} + 2k_c [a_l \sin(\alpha - \beta) - a_u \sin(\alpha + \beta)]\} \tag{4.6a}$$

$$\frac{d\alpha}{d\tau} = -\frac{k_c}{A} \{a_l \cos(\alpha - \beta) - a_u \cos(\alpha + \beta)\}. \tag{4.6b}$$

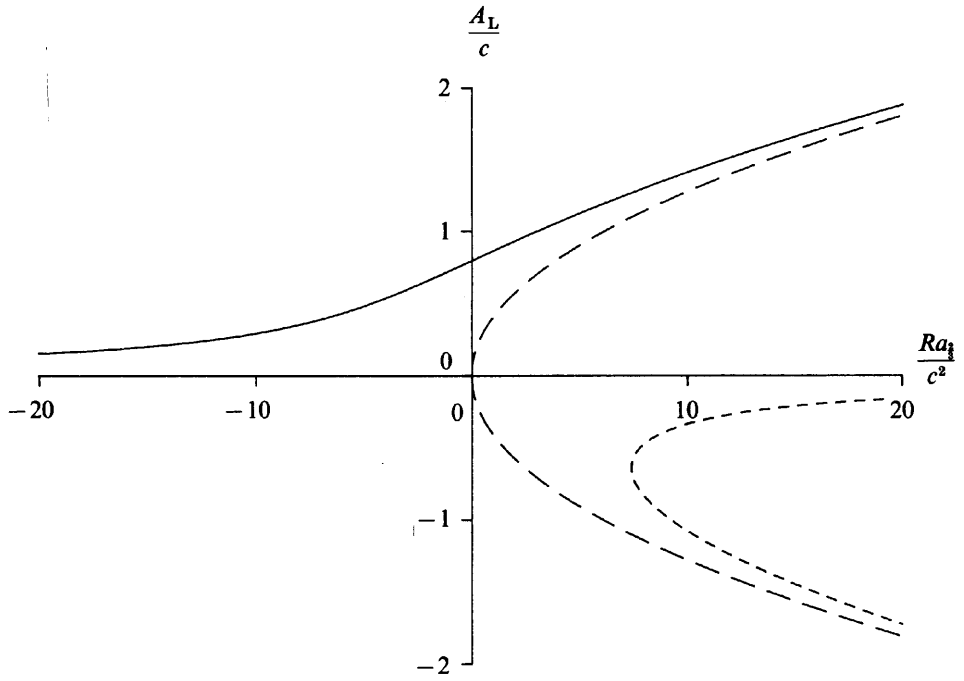

FIGURE 4. The imperfect bifurcation for the general undulating layer (equation 4.5): ——, stable solution; ---------, unstable solutions; – – – – – –, the perfect bifurcation, for reference.

Here (4.6*a*) follows in the same way as (4.5*a*), whilst (4.6*b*) follows by applying the same procedure as for (4.6*a*) but using eigensolutions $\Psi_{\frac{1}{3}}$ and $\Theta_{\frac{1}{3}}$ with phase $\alpha+\frac{1}{2}\pi$ rather than α in the ξ-direction. The equilibrium phase α_p is determined by simply taking $\mathrm{d}\alpha/\mathrm{d}\tau = 0$, hence

$$\tan\alpha_p = \left(\frac{a_u - a_l}{a_u + a_l}\right)\cot\beta. \tag{4.7}$$

Denoting c by c_p when $\alpha = \alpha_p$ in (4.5*b*) and setting $\alpha = \alpha_p + \tilde{\alpha}$ in (4.6*b*) gives

$$\frac{\mathrm{d}\tilde{\alpha}}{\mathrm{d}\tau} = -\frac{k_c}{A}c_p^3 \sin\tilde{\alpha}, \tag{4.8}$$

from which we infer that the solutions along the lower branches are unstable to perturbations that are out of phase with themselves. A linear stability analysis of the upper-branch solutions shows that this branch is stable.

Finally, the effects of detuning may be investigated. Letting

$$k = k_c(1+\delta^{\frac{1}{3}}\tilde{k}) \tag{4.9}$$

be the wall wavenumber and proceeding as above, we find that equation (4.6*a*) is replaced by

$$\frac{\mathrm{d}A}{\mathrm{d}\tau} = -\tfrac{1}{2}[k_c^4 A^3 + (Ra_c\tilde{k}^2 - Ra_{\frac{1}{3}})A + 2k_c(a_l \sin(\alpha-\beta) - a_u \sin(\alpha+\beta))] \tag{4.10}$$

and all the above observations regarding stability remain valid.

4.2. *Three-dimensional*

In other situations, it is known that (i) longitudinal rolls are generated before transverse rolls (Walton 1983)† and (ii) longitudinal rolls are unstable to disturbances

† Walton's definition of a transverse roll is equivalent to our longitudinal roll.

in the form of transverse rolls (Straus 1974). It is of interest therefore to investigate the interaction of longitudinal and transverse modes.

Of course, we must abandon the stream-function description of the problem and adopt a full three-dimensional form. We have found it convenient to work in terms of the pressure. By taking the divergence of (2.1) and substituting for $\boldsymbol{q}$ from (2.1) into (2.3), we obtain

$$\nabla^2 p = Ra\,\theta_z, \tag{4.11}$$

$$\nabla^2\theta = Ra\,\theta\theta_z - \nabla p\cdot\nabla\theta + \frac{\partial\theta}{\partial t}, \tag{4.12}$$

where ∇^2 denotes the three-dimensional Laplacian in x, y, z. The boundaries are impermeable and isothermal, hence

$$\left.\begin{aligned}(\nabla p - Ra\,\theta\hat{\boldsymbol{z}})\cdot\boldsymbol{n} &= 0\\ \theta &= -1\end{aligned}\right\} \quad \text{on } z = 1+\delta g_{\mathrm{u}}(x), \tag{4.13}$$

$$\left.\begin{aligned}(\nabla p - Ra\,\theta\hat{\boldsymbol{z}})\cdot\boldsymbol{n} &= 0\\ \theta &= 1\end{aligned}\right\} \quad \text{on } z = -1-\delta g_{\mathrm{l}}(x), \tag{4.14}$$

where $\boldsymbol{n}$ denotes the normal to the wavy boundary. We recast these equations using new independent variables (ξ, ζ, η), where (ξ, η) are as defined in (3.7) and $\zeta = y$:

$$\left\{\mathrm{L}_1 + s_1^2\frac{\partial^2}{\partial\zeta^2}\right\}p = 2Ra\,s_1\frac{\partial\theta}{\partial\eta}, \tag{4.15}$$

$$\begin{aligned}\left\{\mathrm{L}_1 + s_1^2\frac{\partial^2}{\partial\zeta^2}\right\}\theta = {} & 2Ra\,s_1\,\theta\frac{\partial\theta}{\partial\eta} - s_1^2\left\{\frac{\partial\theta}{\partial\xi}\frac{\partial p}{\partial\xi} + \frac{\partial\theta}{\partial\zeta}\frac{\partial p}{\partial\zeta}\right\}\\ & - \delta s_1 s_2\left\{\frac{\partial\theta}{\partial\eta}\frac{\partial p}{\partial\xi} + \frac{\partial\theta}{\partial\xi}\frac{\partial p}{\partial\eta}\right\} - (4+\delta^2 s_2^2)\frac{\partial\theta}{\partial\eta}\frac{\partial p}{\partial\eta} + s_1^2\frac{\partial\theta}{\partial t},\end{aligned} \tag{4.16}$$

with

$$\left.\begin{aligned}(2-\delta^2 s_2 g_{\mathrm{u}}')\frac{\partial p}{\partial\eta} - \delta s_1 g_{\mathrm{u}}'\frac{\partial p}{\partial\xi} + Ra\,s_1 &= 0\\ \theta &= -1\end{aligned}\right\} \quad \text{on } \eta = 1 \tag{4.17a}$$

$$\left.\begin{aligned}(2+\delta^2 s_2 g_{\mathrm{l}}')\frac{\partial p}{\partial\eta} + \delta s_1 g_{\mathrm{l}}'\frac{\partial p}{\partial\xi} - Ra\,s_1 &= 0\\ \theta &= 1\end{aligned}\right\} \quad \text{on } \eta = -1. \tag{4.17b}$$

We expand

$$p = -\tfrac{1}{2}Ra_{\mathrm{c}}\,\eta^2 + \delta^{\frac{1}{3}}p_{\frac{1}{3}} + \delta^{\frac{2}{3}}p_{\frac{2}{3}} + \dots, \tag{4.18a}$$

$$\theta = -\eta + \delta^{\frac{1}{3}}\theta_{\frac{1}{3}} + \delta^{\frac{2}{3}}\theta_{\frac{2}{3}} + \dots, \tag{4.18b}$$

$$Ra = Ra_{\mathrm{c}} + \delta^{\frac{2}{3}}\mu + \dots, \tag{4.18c}$$

$$k = k_{\mathrm{c}}(1 + \delta^{\frac{1}{3}}\tilde{k} + \dots), \tag{4.18d}$$

where the leading-order terms in the p- and θ-expansions are the conduction-state distributions for plane boundaries. At $O(\delta^{\frac{1}{3}})$ we obtain the usual linear Lapwood equations, but recast due to the (p, θ)-formulation:

$$\nabla^2 p_{\frac{1}{3}} = Ra_{\mathrm{c}}\frac{\partial\theta_{\frac{1}{3}}}{\partial\eta}, \tag{4.19a}$$

$$\nabla^2\theta_{\frac{1}{3}} = -Ra_{\mathrm{c}}\,\theta_{\frac{1}{3}} + \frac{\partial p_{\frac{1}{3}}}{\partial\eta}, \tag{4.19b}$$

with

$$\frac{\partial p_{\frac{1}{3}}}{\partial \eta} = 0, \quad \theta_{\frac{1}{3}} = 0 \quad \text{on } \eta = \pm 1. \tag{4.19c}$$

We concentrate on the eigensolution representing a sum of longitudinal and transverse rolls. On expanding the eigensolution for small δ and truncating at leading order, we have

$$p_{\frac{1}{3}} = [2k_c \sin(k\xi+\alpha) \sin k_c \eta]\, A_L + [2k_c \sin k_c \zeta \sin k_c \eta]\, A_T, \tag{4.20a}$$

$$\theta_{\frac{1}{3}} = [\sin(k\xi+\alpha) \cos k_c \eta]\, A_L + [\sin k_c \zeta \cos k_c \eta]\, A_T, \tag{4.20b}$$

where A_L, A_T denote the amplitudes of the longitudinal and transverse rolls respectively. At $O(\delta^{\frac{2}{3}})$, we obtain the solutions

$$p_{\frac{2}{3}} = -\tfrac{1}{2}k_c^2 [A_L^2 + A_T^2] \cos 2k_c \eta - 2k_c \tilde{k} A_L \cos(k\xi+\alpha) \sin k_c \eta - \tfrac{1}{2}\mu\eta^2 - \tfrac{4}{7}k_c^2 A_L A_T \sin(k\xi+\alpha) \sin k_c \zeta \cos 2k_c \eta, \tag{4.21a}$$

$$\theta_{\frac{2}{3}} = \tfrac{1}{4}k_c [A_L^2 + A_T^2] \sin 2k_c \eta + \tfrac{3}{7}k_c A_L A_T \sin(k\xi+\alpha) \sin k_c \zeta \sin 2k_c \eta, \tag{4.21b}$$

whilst the existence of a solution to the $O(\delta)$ equations requires

$$\frac{dA_L}{d\tau} = \tfrac{1}{2}(\mu - \tilde{k}^2 Ra_c) A_L - \tfrac{1}{2}k_c^4 A_L^3 - \tfrac{5}{7}k_c^4 A_L A_T^2 + k_c c_p^3 \cos\tilde{\alpha}, \tag{4.22a}$$

$$\frac{dA_T}{d\tau} = \tfrac{1}{2}\mu A_T - \tfrac{1}{2}k_c^4 A_T^3 - \tfrac{5}{7}k_c^4 A_L^2 A_T, \tag{4.22b}$$

$$\frac{d\tilde{\alpha}}{d\tau} = -\frac{k_c}{A_L} c_p^3 \sin\tilde{\alpha}. \tag{4.22c}$$

Here we have again set $\alpha = \alpha_p + \tilde{\alpha}$, where α_p is the equilibrium phase, given by (4.7). We now consider the stability of the upper branch of (4.5*a*) to cross-roll disturbances. On substituting $(A_L, A_T, \tilde{\alpha}) = (A, 0, 0) + (A_L', A_T', \alpha')$ and linearizing, we obtain

$$\frac{dA_L'}{d\tau} = \tfrac{1}{2}[\mu - \tilde{k}^2 Ra_c - 3k_c^4 A^2] A_L', \tag{4.23a}$$

$$\frac{dA_T'}{d\tau} = \tfrac{1}{2}[\mu - \tfrac{10}{7}k_c^4 A^2] A_T', \tag{4.23b}$$

$$\frac{d\alpha'}{d\tau} = -\frac{k_c c_p}{A} \alpha'. \tag{4.23c}$$

For the stability of the upper-branch solutions, both terms in the square brackets in (4.23) must be negative. Hence the curve of marginal stability is given by $\mu = \frac{10}{7}k_c^4 A^2$, which intersects the upper branch at the positive roots of

$$\tfrac{3}{10}\mu^{\frac{3}{2}} - Ra_c \tilde{k}^2 \mu^{\frac{1}{2}} + 2(\tfrac{10}{7})^{\frac{1}{2}} k_c^3 c_p^3 = 0. \tag{4.24}$$

The maximum detuning allowable in order that the whole of the upper branch be stable is easily determined to be $\tilde{k}_{max}$, where

$$|\tilde{k}_{max}| = \frac{9^{\frac{1}{3}}}{7^{\frac{1}{6}}} \frac{k_c c_p}{Ra_c^{\frac{1}{2}}} = 0.75197 c_p, \tag{4.25a}$$

at which point

$$\mu_{max} = \frac{10}{(63)^{\frac{1}{3}}} k_c^2 c_p^2. \tag{4.25b}$$

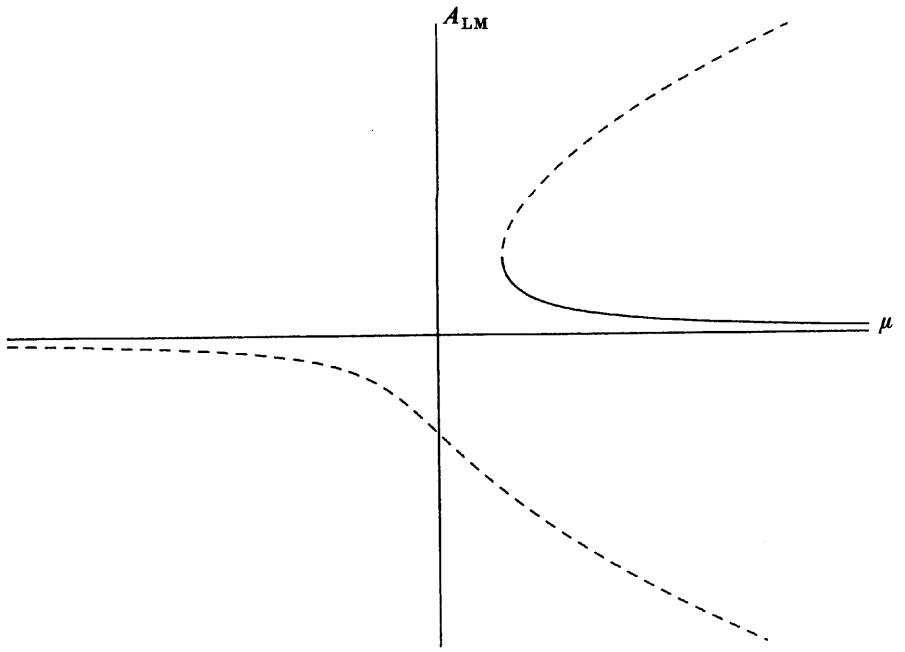

FIGURE 5. A sketch of the longitudinal component of the mixed mode for the general undulating layer (equation 4.26): ——, stable solution; ---------, unstable solution.

We note that the pure A_L mode is stable for high enough values of μ, irrespectively of the degree of detuning within the $O(\delta^{\frac{1}{3}})$ range.

The pure A_L mode, however, is not the only equilibrium state: there exists a mixed-mode solution to (4.22) with $A_T \neq 0$. On eliminating A_T, the longitudinal component A_{LM} of the mixed mode satisfies

$$\tfrac{17}{7}k_c^4 A_{LM}^3 - [\mu + \tfrac{7}{3}\tilde{k}^2 Ra_c] A_{LM} + \tfrac{14}{3}k_c c_p^3 = 0. \tag{4.26}$$

A sketch of A_{LM} is displayed in figure 5. A stability analysis reveals that the upper and lower branches are both unstable, whilst the middle branch is stable. It should be emphasized that there is no pure A_T mode solution to (4.23) and so transverse rolls cannot constitute the most unstable mode.

By considering the condition for the existence of the transverse component of the mixed-mode (i.e. from (4.22*b*)), we deduce that the roots of (4.24) coincide with the points where the A_{LM} mode curve intersects the A_L mode curve. The situation is illustrated qualitatively in figure 6 for various $\tilde{k}$. For the purposes of delineating the three possible regimes, we introduce the value $\tilde{k}_{min}$, via

$$|\tilde{k}_{min}| = \left(\frac{51}{49}\right)^{\frac{1}{6}}\left(\frac{41}{68}\right)^{\frac{1}{2}} c_p = (0.7817 c_p), \tag{4.27}$$

which is the amount of detuning needed for the stable middle branch of the A_{LM} mode to intersect the stable upper branch of the A_L mode. For $|\tilde{k}| < |\tilde{k}_{max}|$, the whole of the upper branch of the A_L mode is stable and there is also a stable mixed-mode solution which exists when $\mu > \hat{\mu}$, where

$$\hat{\mu} = (357)^{\frac{1}{3}} k_c^2 c_p^2 - \tfrac{7}{3}\tilde{k}^2 Ra_c. \tag{4.28}$$

For $|\tilde{k}_{max}| < |\tilde{k}| < |\tilde{k}_{min}|$ there is a sub-interval in which the A_L mode is unstable, whilst the mixed-mode is stable. Finally, when $|\tilde{k}| > |\tilde{k}_{min}|$, there is a continuous transition from the A_L mode to the mixed mode.

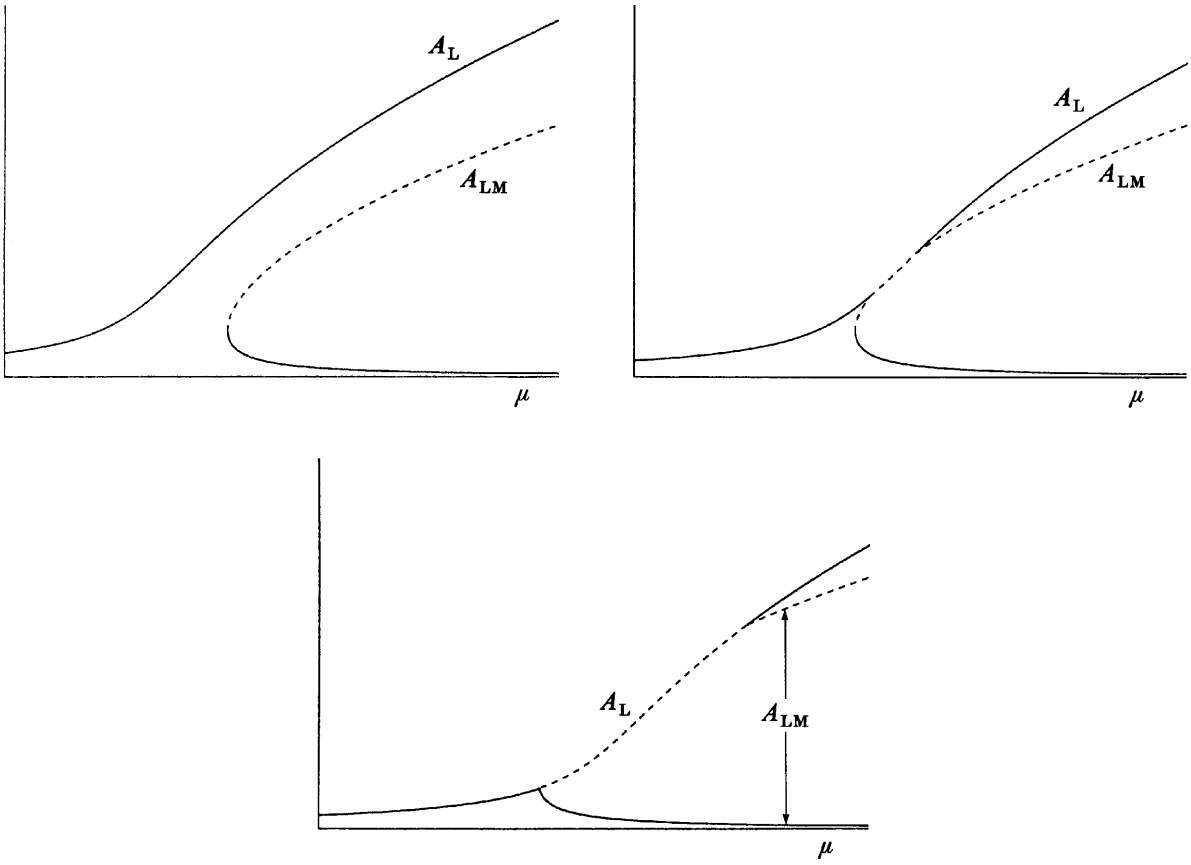

FIGURE 6. An illustration of the three possible regimes for the stability and existence of longitudinal and mixed modes for the general undulating layer: ——, stable solutions; ---------, unstable solutions.

5. The critical regime for the varicose configuration

We turn now to the special case mentioned in §3, namely the varicose configuration with $a_l = a_u = a$ and $\beta = 0$. In this case, expansion (3.10) remains regular near $Ra = Ra_c$ but the solution that it represents becomes unstable. We have what Tavantzis *et al.* (1978) call a *weak* imperfection: the imperfection modifies, but does not alter the qualitative character of the bifurcation.

We first determine the critical Rayleigh number for longitudinal rolls and then consider the interaction of longitudinal and transverse rolls. We shall see that, in contrast to the non-varicose case, transverse rolls are the first to appear but that at higher Rayleigh numbers both longitudinal rolls and transverse rolls are possible stable modes (at least to the types of disturbance considered here).

5.1. *Two-dimensional*

For $k = k_c$ and $Ra \sim Ra_c$, we assume the double expansions

$$(\psi, \theta, Ra) = \sum_{m=0}^{\infty} \sum_{n=0}^{\infty} \epsilon^m \delta^n (\psi_{mn}, \theta_{mn}, Ra_{mn}), \tag{5.1}$$

where ϵ, the scale of the convection amplitude, is regarded as small and

$$(\psi_{00}, \theta_{00}, Ra_{00}) = (0, -\eta, Ra_c). \tag{5.2}$$

As both δ and Ra are externally imposed parameters, (5.1) actually defines ϵ.

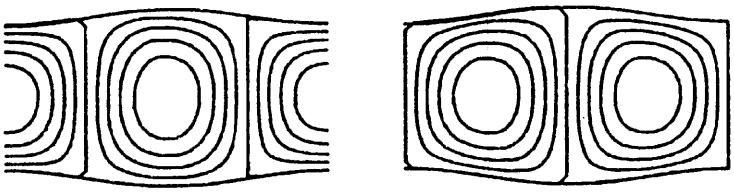

(a) (b)

FIGURE 7. The streamlines (equation 5.3) of the two-dimensionally stable mildly supercritical roll solutions for the varicose layer: (a) $\alpha = n\pi$ (infinite layer); (b) $\alpha = (n+\frac{1}{2})\pi$ (infinite cylinder).

From the work of Palm *et al.* on weakly nonlinear Lapwood convection, we deduce that $Ra_{10} = 0$, $Ra_{20} = k_c^4$ and

$$(\psi_{01}, \theta_{01}) = (-2k_c \cos(k_c\xi+\alpha)\cos k_c\eta, \sin(k_c\xi+\alpha)\cos k_c\eta), \tag{5.3}$$

where α is an arbitrary phase. After much tedious analytical work, we further find that $Ra_{01} = Ra_{11} = 0$ (as expected on symmetry considerations) and

$$\frac{Ra_{02}}{a^2} = \left[1+\frac{1}{4\sinh^2\sqrt{3}\,k_c}\right]k_c^4+\left[\frac{1}{\sqrt{3}}\coth\sqrt{3}k_c\right]k_c^3 + \left[\frac{\sqrt{3}}{12}\coth\sqrt{3}k_c-\frac{k_c}{4}\right]k_c^3\cos 2\alpha. \tag{5.4}$$

As Ra_{02} is dependent on α, the preferred phase must be determined as in §4.1. Applying the solvability condition on the $O(\epsilon\delta^2)$ equations yields

$$\frac{d\alpha}{d\hat{\tau}} = -\frac{1}{8}\left[k_c-\frac{1}{\sqrt{3}}\coth\sqrt{3}k_c\right]k_c^3\sin 2\alpha, \tag{5.5}$$

where the term in square brackets is positive and $\hat{\tau} = \delta^2 t$. The preferred phases are given by $\alpha = n\pi$ for integer n, which correspond to rolls centred in the hollows and constrictions. These rolls have critical Rayleigh number

$$Ra = Ra_c + 7.4141a^2\delta^2 + O(\delta^4). \tag{5.6}$$

The other equilibrium solutions of (5.5), namely $\alpha = (n+\frac{1}{2})\pi$, are also of interest. For although they give rolls which are unstable in the infinite layer, they are stable when there is any vertical insulated barrier positioned symmetrically in the varicose undulations, i.e. at $\xi = 2n_1$ for some integer n_1. The corresponding critical Rayleigh number for this case is

$$Ra = Ra_c + 9.3796a^2\delta^2 + O(\delta^4). \tag{5.7}$$

The two cases described above are illustrated in figure 7. For convenience we call the stable flow with $\alpha = n\pi$, type I and that with $\alpha = (n+\frac{1}{2})\pi$, type II.

The effects of detuning are such that the critical Rayleigh numbers for type-I and -II modes are both increased by an amount $\delta^2\tilde{\tilde{k}}^2 Ra_c$, when the wall wavenumber is $k = k_c(1+\delta\tilde{\tilde{k}})$. The conclusions regarding stability remain valid.

5.2. *Three-dimensional*

Here we consider the varicose analogue of §4.2. The governing equations are (4.15)–(4.17), where g_u and g_l are given by (3.6) with $k = k_c$, $a_u = a_l = a$ and $\beta = 0$. In order to incorporate the fully interactive three-dimensional case, we assume that

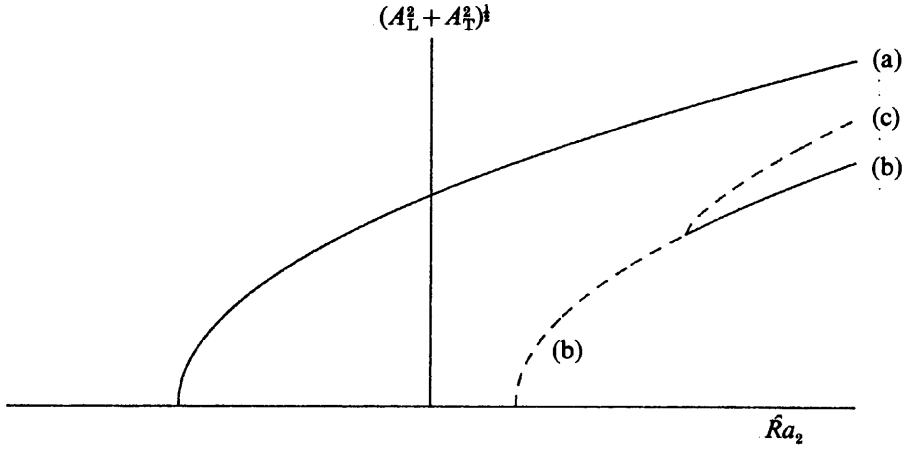

FIGURE 8. Sketch of the primary and secondary bifurcation for the varicose layer. (*a*) transverse rolls, (*b*) longitudinal rolls, (*c*) mixed mode.

the convective rolls have amplitudes which are $O(\delta)$. Thus, for $Ra \sim Ra_c$, we assume that

$$(p, \theta, Ra) = \sum_{n=0}^{\infty} \delta^n(\hat{p}_n, \hat{\theta}_n, \hat{Ra}_n), \tag{5.8}$$

where

$$(\hat{p}_0, \hat{\theta}_0, \hat{Ra}_0) = (-\tfrac{1}{2}Ra_c\,\eta^2, -\eta, Ra_c). \tag{5.9}$$

At $O(\delta)$, we take

$$\hat{p}_1 = \hat{h}(\eta)\cos k_c\,\xi + 2k_c[\hat{A}_L \sin(k_c\,\xi+\alpha) + \hat{A}_T \sin k_c\,\zeta]\sin k_c\,\eta, \tag{5.10a}$$

$$\hat{\theta}_1 = \hat{g}(\eta)\cos k_c\,\xi + [\hat{A}_L \sin(k_c\,\xi+\alpha) + \hat{A}_T \sin k_c\,\zeta]\cos k_c\,\eta, \tag{5.10b}$$

where

$$\hat{h}(\eta) = -4k_c^2\,\eta^2 - k_c\cos k_c\,\eta + \sqrt{3}k_c\frac{\cosh\sqrt{3}k_c\,\eta}{\sinh\sqrt{3}k_c}, \tag{5.11a}$$

$$\hat{g}(\eta) = \frac{1}{2}\left[\sin k_c\,\eta + \frac{\sinh\sqrt{3}k_c\,\eta}{\sinh\sqrt{3}k_c} - 2\eta\right] \tag{5.11b}$$

and $\hat{A}_L$, $\hat{A}_T$ denote the amplitudes of the longitudinal and transverse rolls respectively. Again omitting all the details, it is found that $\hat{Ra}_1 = 0$ and

$$\frac{d\hat{A}_L}{d\hat{\tau}} = \tfrac{1}{2}\hat{A}_L[\hat{Ra}_2 - \hat{Ra}_L - k_c^4\,\hat{A}_L^2 - \tfrac{10}{7}k_c^4\,\hat{A}_T^2], \tag{5.12a}$$

$$\frac{d\hat{A}_T}{d\hat{\tau}} = \tfrac{1}{2}\hat{A}_T[\hat{Ra}_2 - \hat{Ra}_T - k_c^4\,\hat{A}_T^2 - \tfrac{10}{7}k_c^4\,\hat{A}_L^2], \tag{5.12b}$$

where $\hat{Ra}_L$ is identical with Ra_{02} given by (5.4) and $\hat{Ra}_T$ is found numerically to have the value $-22.504a^2$; the equation for the phase α is again given by (5.5). A stability analysis shows that the longitudinal mode with $\alpha = (n+\frac{1}{2})\pi$ is unstable, whilst the pure transverse mode is stable. For $\hat{Ra}_2 > \hat{Ra}_L$ there is also a longitudinal mode with $\alpha = n\pi$, which is unstable until it suffers a secondary bifurcation to an unstable mixed mode at

$$\hat{Ra}_2 = \tfrac{1}{3}[10\hat{Ra}_L - 7\hat{Ra}_T], \tag{5.13}$$

see figure 8. For an infinite cylinder formed by inserting vertical insulated boundaries into the infinite varicose layer as described in §5.1, type II is the only possible longitudinal mode. Its bifurcation diagram has the same form as in figure 8, but with $\hat{Ra}_L$ having the appropriate value.

6. Numerical solution: varicose configuration

Thus far, we have concentrated upon the stability of longitudinal and transverse rolls in a slightly undulating layer. The asymptotic solutions that we have found are valid for small boundary amplitudes and for Rayleigh numbers varying from zero to slightly supercritical, i.e. $Ra \lesssim Ra_c$. In order to obtain two-dimensional solutions for finite wall amplitude and for larger Rayleigh numbers, we have made recourse to numerical techniques.

The first numerical study of supercritical motion in the plane porous layer was made by Elder (1967), who calculated finite-difference solutions with which to compare his experimental results. Elder restricted his attention to two-dimensional roll solutions with wavenumber k_c; stability with respect to three-dimensional disturbances was not considered. Straus (1974), using a Galerkin method, considered general disturbances and showed that, at a given value of the Rayleigh number, stable two-dimensional flow is possible for a finite band of horizontal wavenumbers provided that $Ra_c \leqq Ra \lesssim 9.5Ra_c$.

Other literature related to the two-dimensional case is concerned with steady and unsteady convection in rectangular boxes: Horne & O'Sullivan (1974, 1978), Caltagirone (1975) and Schubert & Straus (1979, 1982). In these studies, the computational region fixes the range of possible wavenumbers. For unicellular convection with wavenumber k_c, the flow is steady for Rayleigh numbers that are mildly supercritical, but eventually becomes oscillatory as the Rayleigh number increases. The critical value for the onset of this fluctuating motion has been variously reported to have a value ranging from about $7Ra_c$ (Horne & O'Sullivan 1974) to about $9.5Ra_c$ (Caltagirone 1975); see Horne (1979) and Schubert & Straus (1982) for interesting discussions. Moreover it appears that all two-dimensional multicellular patterns of convection become oscillatory with increasing Rayleigh number and the larger the number of cells is, the higher is the value of Ra at the onset of oscillatory behaviour (Schubert & Straus 1979).

When the effects of boundary variations are included in the numerical analysis, we shall see that there is a stabilization to the convective instability and also that the flow becomes oscillatory at much lower Rayleigh numbers. We have found three distinct types of periodic motion depending upon the exact configuration and upon the boundary amplitude and Rayleigh number.

We consider only two-dimensional convection in a varicose layer with $k = k_c$, as this is a relatively simple but interesting case to study. The numerical study of Straus (1974) concerning the stability of rolls to three-dimensional disturbances in the Lapwood problem shows that rolls with wavenumber k_c are stable up to about $5Ra_c$. Whilst recognizing that the roll-stability region of Straus will be modified by the presence of boundary undulations, we expect that, if these undulations are small, there will be Rayleigh numbers for which stable longitudinal rolls are realizable physically. Furthermore, the stability analysis of §5 indicates that for large enough Rayleigh number both longitudinal and transverse rolls may exist and are stable. In view of figure 8, it seems more likely that transverse rolls will be observed. However, for a layer that is of finite extent in the y-direction, with vertical insulated boundaries that are not an integer multiple of the critical cell width ($\pi/k_c = 2$) apart, we can show that stable longitudinal rolls appear at a lower Rayleigh number than transverse rolls. Geophysically this situation could occur where an undulating rock stratum is bounded by vertical faults. In view of this latter observation, we consider

a two-dimensional study not only to be a starting point for a full three-dimensional study, but also worthwhile in its own right.

The governing nonlinear time-dependent equations (3.8), (3.9) with $\delta = 1$ and $a_u = a_l = a$ were discretized using a uniform square grid. The solution domain consisted of one wavelength of the varicose layer or, equivalently, a 4×2 rectangle in the transformed (ξ, η)-plane. The Dufort–Fraenkel scheme was used for the temporal and diffusion terms in (3.9), whilst a second-order Arakawa method (1966) was used for the advection terms. Roache (1972) points out that the conservation properties of the Arakawa scheme make it ideally suited to hydrodynamic stability problems.

The stream-function equation (3.8) was discretized using second-order central-difference approximations. For a given temperature field, the resulting linear equations were solved by successive over-relaxation with an optimum relaxation parameter which varied little for the range of amplitudes considered. Due to the presence of single and mixed derivatives in the transformed Laplacian, the iteration matrix lacked diagonal dominance, but no consequential difficulties with convergence were experienced. To accelerate the convergence, a pointwise quadratic extrapolation procedure was employed to provide an initial iterate. On testing the program, it was found necessary to ensure high accuracy in the solution to (3.8) in order to avoid a time-splitting instability in the solution to (3.9).

A grid of 41×21 points was used with a mesh length of 0.1. The time step varied between 0.0025 and 0.01 depending on whether the flow was steady or not, and on the Rayleigh number. Starting with either the conduction solution or a converged temperature field from a neighbouring parameter case, (3.8) was solved to determine a stream function ψ. This was then used in (3.9) and the temperature distribution updated. This process was iterated until a pointwise convergence criterion was satisfied by the stream function.

Various checks were first made in order to verify the numerical procedure. First the Lapwood problem was considered. It was found that:

(i) the critical Rayleigh number was 9.95, an error of less than 1 %;

(ii) the supercritical growth rate was almost exactly $\frac{1}{2}(Ra - Ra_c)$;

(iii) the heat-transfer results were in good agreement with those of Elder (1967).

The results of Straus (1974) are dependent on the roll wavenumbers, which were chosen to maximize the heat transfer at any given Rayleigh number, and in consequence they are in an inconvenient form for easy comparison. Secondly, the subcritical heat transfer for $a = 0.1$ was calculated and found to be in close agreement with that given by (3.18a, b).

We shall present numerical results for two cases, which are related to the type-I and type-II modes introduced in §5.1. The first type corresponds to stable flows in infinite layers, whilst the second corresponds to stable flows in, say, infinite cylinders. For type I flows the full 41×21 computational grid was used, whereas for type II flows it was reduced to 21×21 by using symmetry about $\xi = 0$.

As the amplitude increases from zero to some small finite value, the analyses of §3 and §5 should give accurate qualitative and quantitative predictions. This is confirmed by the numerical results. In particular, for low Rayleigh numbers, the only flow that we could determine numerically was a weak convection consisting of four cells, which corresponds to the quasi-conduction flow discussed in §3. For higher Rayleigh numbers this flow became unstable and bifurcated supercritically into strongly convecting steady two-cell solutions, thus confirming the results in §5.1. In

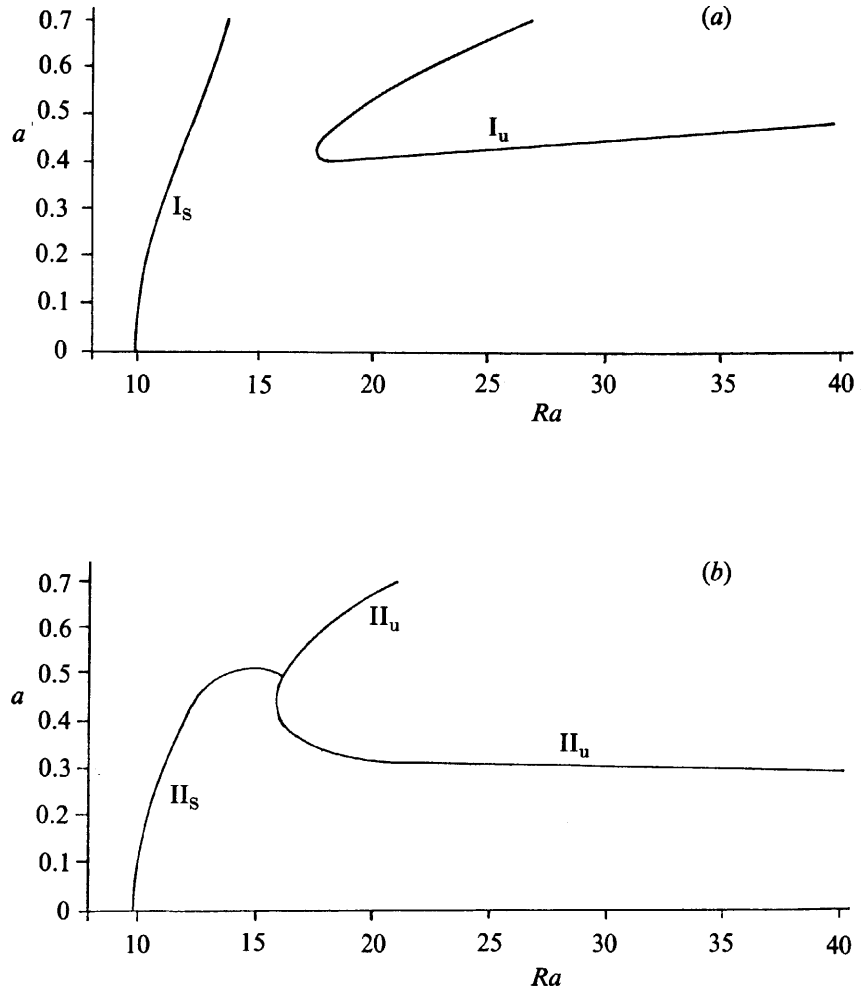

FIGURE 9. The marginal stability curves for (*a*) the infinite layer (I_S) and (*b*) the infinite cylinder (II_S), as determined by numerical experiment. Also shown are the respective boundaries I_u, II_u between steady and periodic flows.

figure 9, we have traced out the curves of marginal stability, labelled I_S and II_S, for type-I and -II modes respectively. On using a non-negative functional $\hat{J}$ which filters out the motion due to the baroclinic effect:

$$\hat{J}^2 = \int_{-1}^{1} \int_{-\pi/k_c}^{\pi/k_c} [\psi(\xi, \eta) + \psi(\xi, -\eta)]^2 \, \mathrm{d}\xi \, \mathrm{d}\eta, \tag{6.1}$$

we find that

$$\hat{J} \propto |Ra - Ra_i|^{\frac{1}{2}}, \tag{6.2}$$

and

$$\hat{J} \propto |a_i - a|^{\frac{1}{2}}, \tag{6.3}$$

where i = I or II. Here $Ra_I(a)$, $Ra_{II}(a)$ are the critical Rayleigh numbers and $a_I(Ra)$, $a_{II}(Ra)$ the critical amplitudes corresponding to the curves I_S, II_S respectively. The behaviours along I_S and II_S as $a \to 0+$ are

$$Ra_I \sim 9.95 + 8.5a^2, \tag{6.4}$$

$$Ra_{II} \sim 9.95 + 9.6a^2, \tag{6.5}$$

which may be compared with the analytical formulae (5.6) and (5.7). On using simple linear extrapolation, it seems that $\lim_{a_I \to 1-} Ra_I = 15.3$ (see figure 9*a*). It should be stressed, however, that our numerical method is not able to deal with the singular limit of upper and lower boundaries touching.

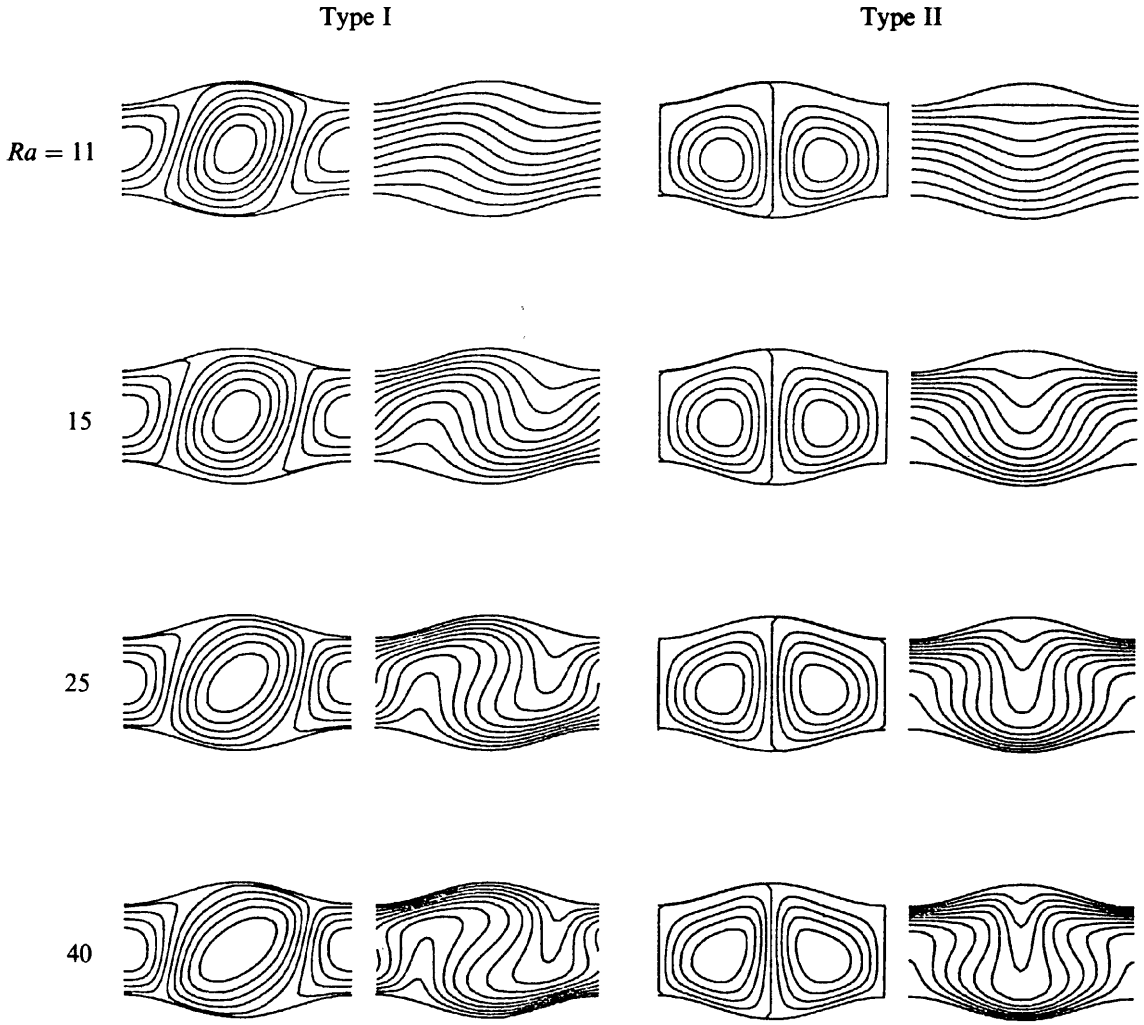

FIGURE 10. Comparison of the types-I and -II solutions for selected Rayleigh numbers at $a = 0.2$. For each pair, the streamlines are on the left and the isotherms on the right – this convention applies also to figures 11, 17, 18 and 19. The streamlines and isotherms are drawn at equal intervals between their respective extrema.

It is of interest to compare the type-I and -II modes as the Rayleigh number increases, and these are shown in figure 10 where we have taken $a = 0.2$ as a typical amplitude. For the infinite layer (shown on the left in figure 10), the large cell in the hollow is always tilted due to the action of aiding buoyancy forces along one half of both boundaries and opposing forces on the other halves. This is in contrast to the Lapwood problem where the streamlines first distort near the centre of the layer as Ra increases (cf. Elder 1967, figure 5). This buoyancy-force action also affects the type-II flow (shown on the right in figure 10), but now produces a vertical asymmetry by opposing the motion along the upper boundary (as we have shown it) and aiding it on the lower. It should be noted that the solutions found by reflecting in $\eta = 0$ those in figure 10 also satisfy (3.8) and (3.9) and are equally likely to occur.

In figure 11, we have shown, for a fixed Rayleigh number, the effects upon the modes of varying the boundary amplitude. As a increases, the strength of the flow decreases until $\mathrm{I_S}$ or $\mathrm{II_S}$ is crossed, at which point the weakly convecting four cell solutions are re-established. This reappearance is not surprising in view of the increased baroclinic effect. A typical plot of the extreme values taken by the stream functions is shown in figure 12; the point of coalescence for the type-I case corresponds to a point on $\mathrm{I_S}$ in figure 9.

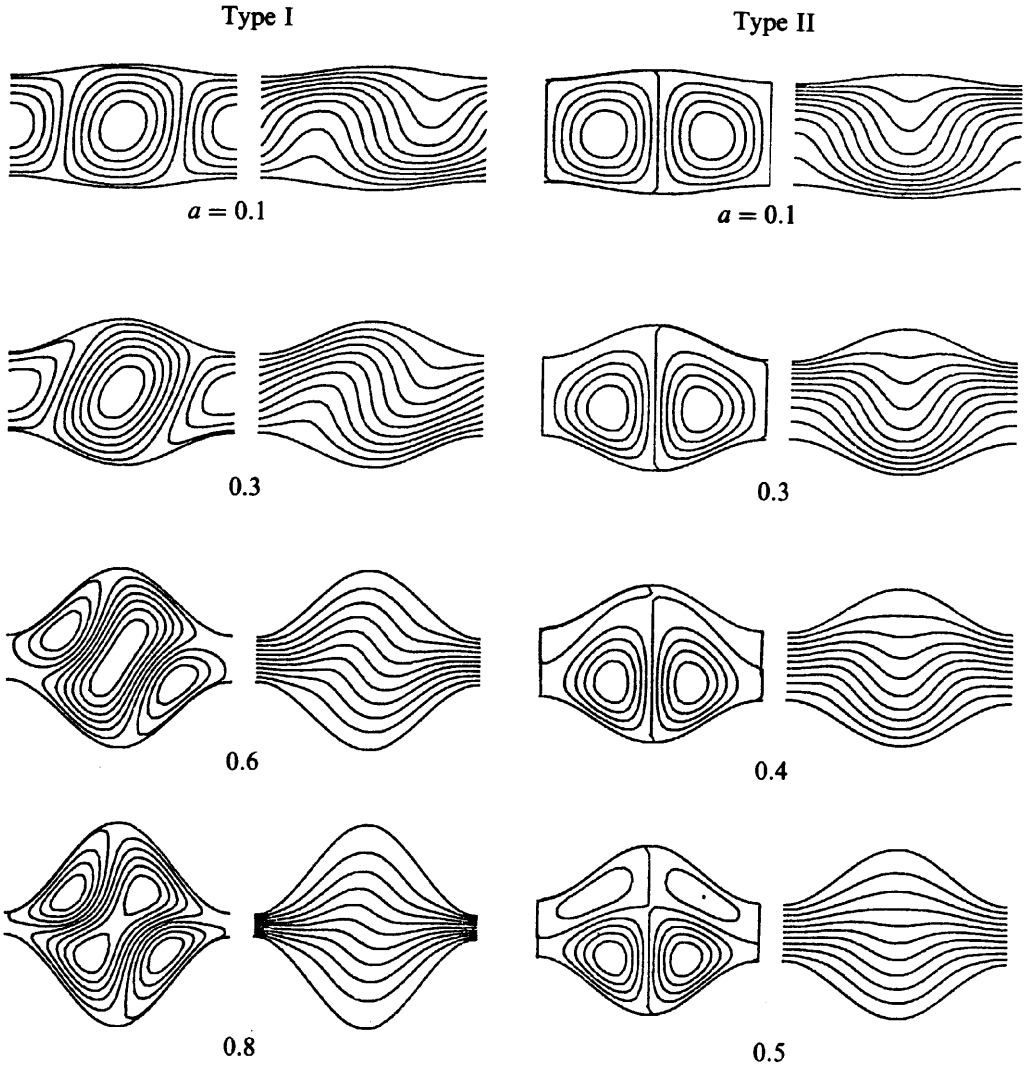

FIGURE 11. Comparison of the types-I and -II solutions for selected wall amplitudes at $Ra = 15$. The streamlines and isotherms are equally spaced.

Heat-transfer results for steady flow are shown in figures 13–15. A plot of $-\overline{Nu}$ as given by (3.17) would not approach unity as $Ra \to 0$ because the resultant value would be for the heat transferred between wavy, rather than plane, boundaries. Thus for a simpler graphical representation, we have plotted

$$Q = \frac{\overline{Nu}(a, Ra)}{\overline{Nu}(a, 0)}. \tag{6.6}$$

A graph of the denominator is shown in figure 13, whilst graphs of Q for modes I and II are shown in figures 14 and 15 respectively. The plots in figures 14 and 15 terminate at either $Ra = 40$ or the occurrence of periodic flow. It is of interest to note that just before the flow becomes oscillatory, the flow strength and heat transfer decrease.

For values of (Ra, a) lying to the right of curves $\mathrm{I_u}$ and $\mathrm{II_u}$ in figure 9, convection ceases to be steady and a periodic flow results. On the lower branch of $\mathrm{II_u}$ and the whole of $\mathrm{I_u}$, the period t_p satisfies

$$t_\mathrm{p} \sim \text{const.}\, |Ra - Ra_\mathrm{u}|^{-\frac{1}{2}} \quad \text{as} \quad Ra \to Ra_\mathrm{u}, \quad \text{fixed}\, a, \tag{6.7}$$

and

$$t_\mathrm{p} \sim \text{const.}\, |a - a_\mathrm{u}|^{-\frac{1}{2}} \quad \text{as} \quad a \to a_\mathrm{u}, \quad \text{fixed}\, Ra, \tag{6.8}$$

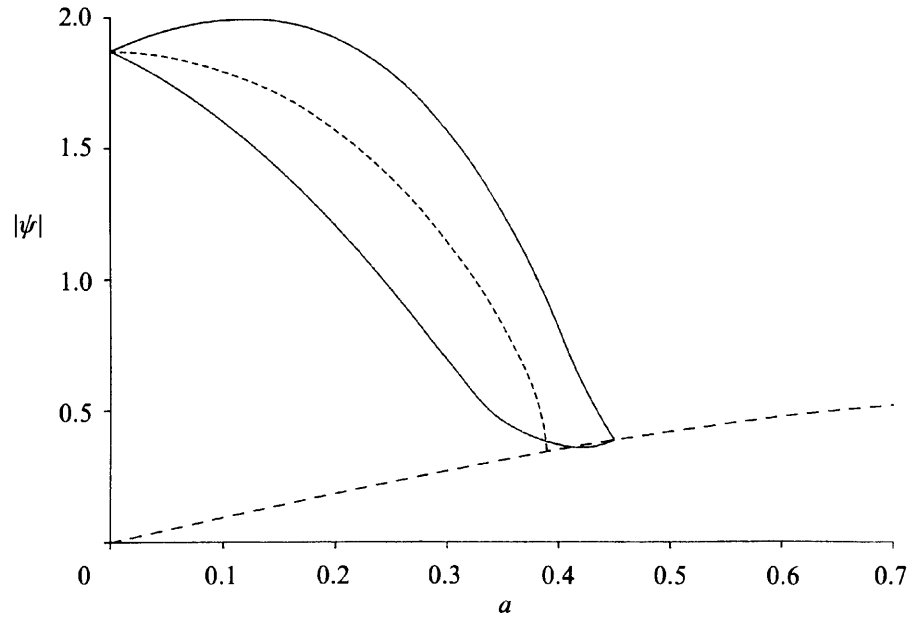

FIGURE 12. Plots of the extreme values taken by the stream function as a function of the wall amplitude a: ——, $\psi_{\max}$ and $-\psi_{\min}$ for type-I flows; ---------, $\psi_{\max}$ for type-II flows; – – – – – –, $\psi_{\max}$ for the weakly convecting solution.

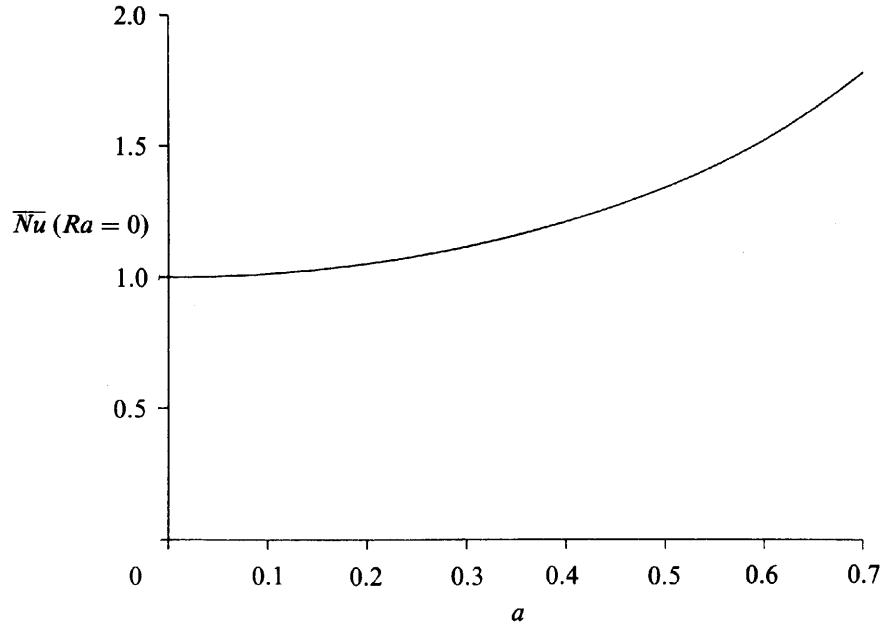

FIGURE 13. The average heat transfer per unit wavelength at $Ra = 0$.

where Ra_u and a_u denote the critical Rayleigh number and critical amplitude for the onset of periodicity at fixed amplitude and Rayleigh number respectively, and where the limits in (6.7) and (6.8) are approached from within the unsteady region. Near the intersection of II_S and II_u, the determination of these curves became difficult due to the presence of both monotonic and oscillatory modes which decay or grow very slowly. Along the upper branch of II_u, the bifurcation is of Hopf type.

The extrema of the stream-function values as a function of time are shown in figure 16 for the three cases: (i) $Ra = 25$, $a = 0.45$, type I (note that for type I flows $|\psi_{\max}|$ is not equal to $|\psi_{\min}|$, in general), (ii) $Ra = 20$, $a = 0.45$, type II and (iii) $Ra = 19$, $a = 0.6$, type II. The corresponding instantaneous streamlines and isotherms are

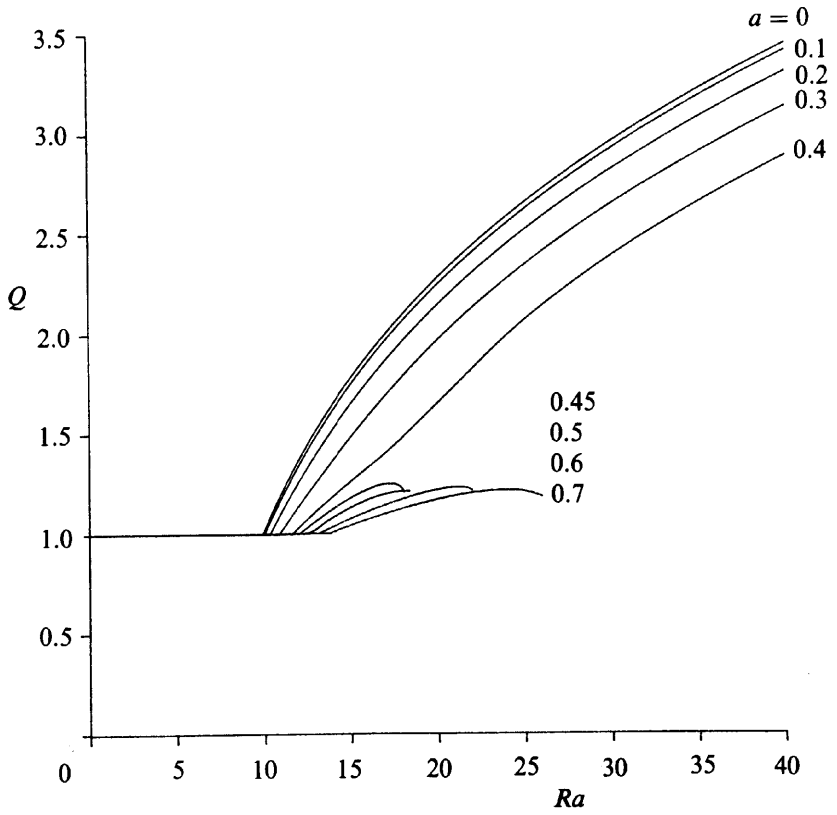

FIGURE 14. The Nusselt number based on the heat transfer at $Ra = 0$ for type-I flows.

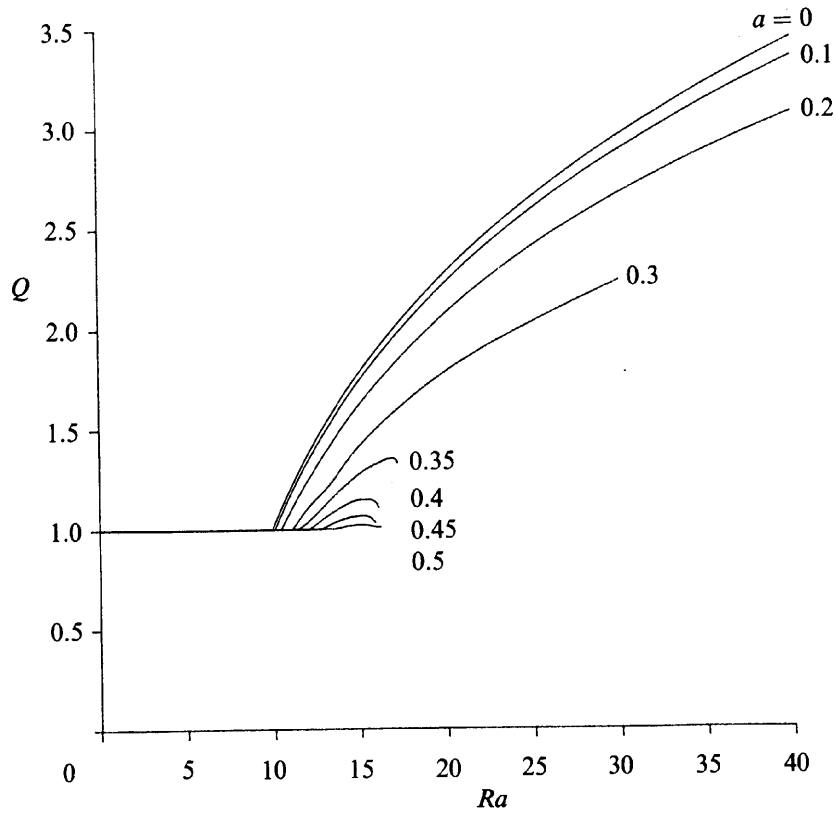

FIGURE 15. The Nusselt number based on the heat transfer at $Ra = 0$ for type-II flows.

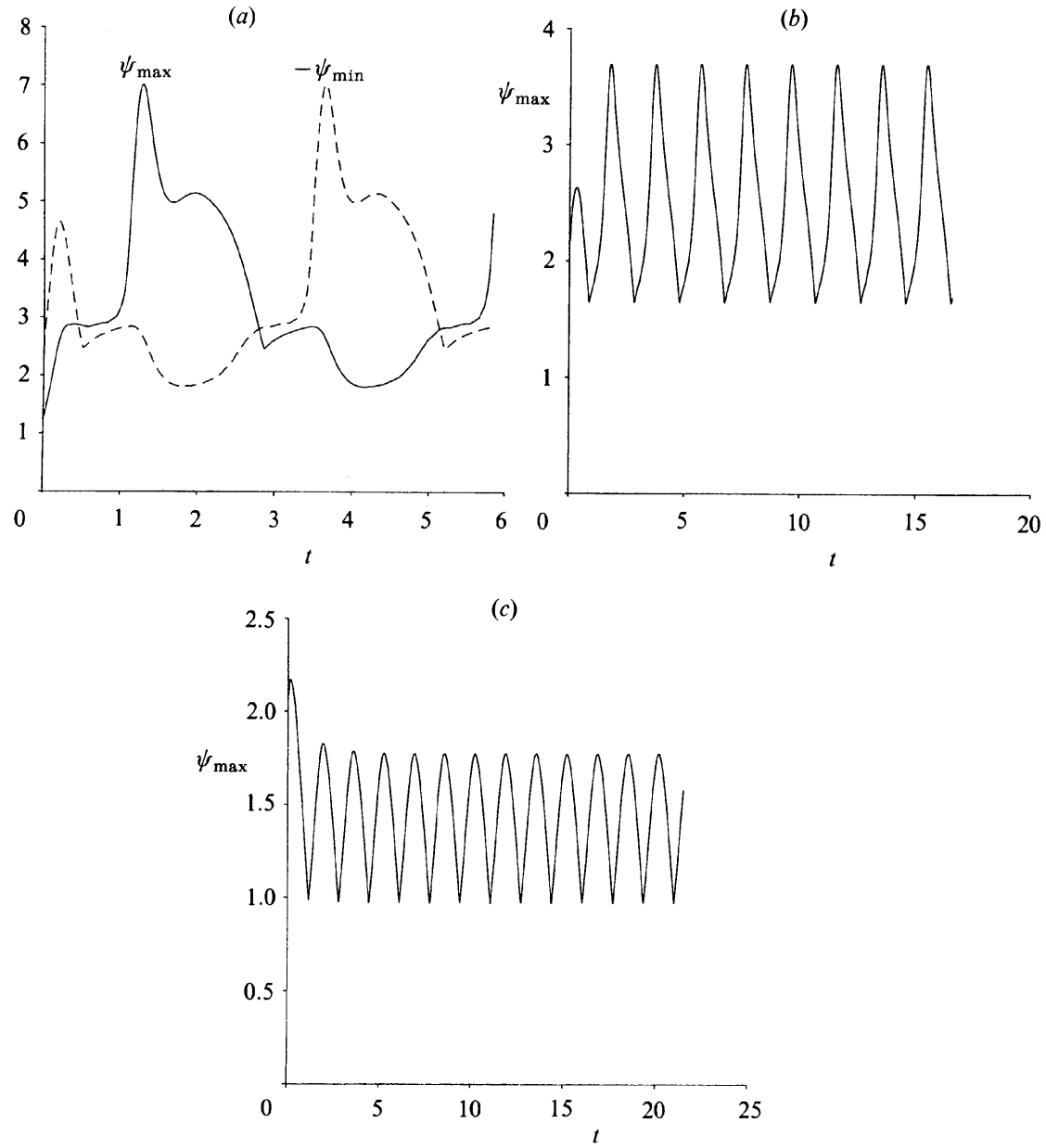

FIGURE 16. Variations of the extreme stream-function values with time: (*a*) ψ_{max} and $-\psi_{min}$ for $Ra = 25$, $a = 0.45$, type I; (*b*) ψ_{max} for $Ra = 20$, $a = 0.45$, type II; (*c*) ψ_{max} for $Ra = 19$, $a = 0.6$, type II.

shown in figures 17–19, where in each of the initial and final plots $|\psi|$ takes on a maximum. The three periodic flows displayed in these figures are representative of all those found in the range of boundary amplitudes and Rayleigh numbers considered.

In figure 17, case (i), the flow is characterized by essentially four phases: the creation of cells in the constrictions, the migration of these cells into the hollows, the merging of the cells and the final dissipation of the resultant cells as the next generation of cells grow and migrate from the constrictions. Note also that the flow changes its sense as the cell in the hollow oscillates, and that there is symmetry in each half-cycle. A similar picture of creation and annihilation of cells is seen in figure 18, case (ii). The main differences for this type-II flow being the symmetry about the vertical centreline, the number of cells and the absence of vortex splitting. Whilst the symmetry and number of cells for case (iii) are similar to case (ii), the character of the oscillatory flow shown in figure 19 is distinct from cases (i) and (ii). The flow

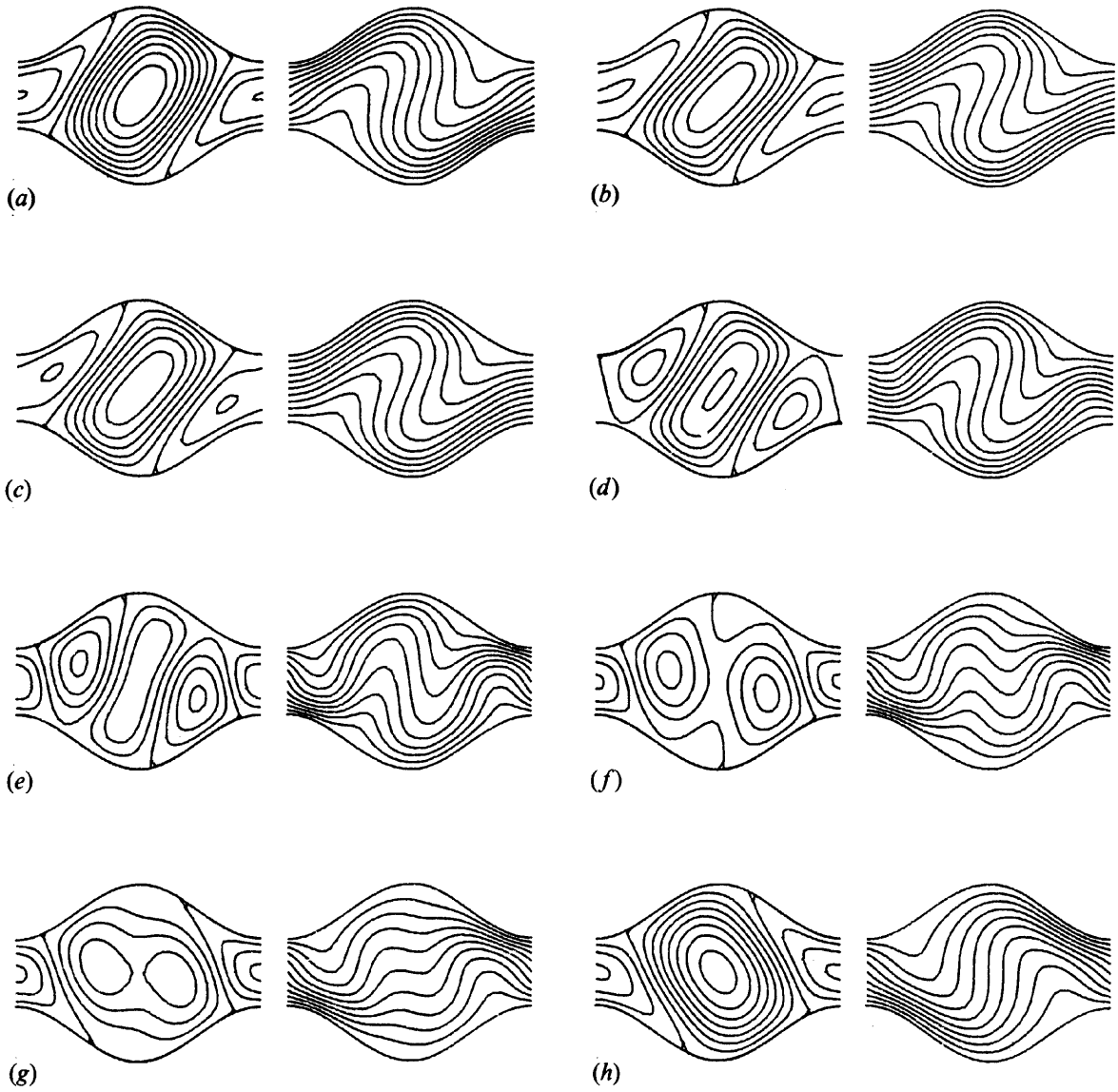

FIGURE 17. Instantaneous streamlines and isotherms for $Ra = 25$, $a = 0.45$, type I, for half a cycle. (*a*) $t = 1.285$, (*b*) 1.67, (*c*) 1.95, (*d*) 2.855, (*e*) 3.25, (*f*) 3.38, (*g*) 3.515, (*h*) 3.645.

is an oscillatory form of the four-cell solution and there is no generation or annihilation of cells.

Finally it is natural to try to relate the three modes of oscillatory flow discussed here with the oscillatory flows that have been determined for configurations with plane sides. Caltagirone (1975) finds a periodic flow which has a pronounced streamline deformation in the centre of the cells. A similar pattern was found by Frick & Müller (1983) in a study of the related problem of unsteady convection in a Hele-Shaw cell heated from below. This particular flow, termed type A by Frick & Müller, is attributed to an instability of the thermal boundary layer, and is quite unlike any of our modes. Frick & Müller also find a second periodic flow, termed type B, which bears certain similarities to our case (i) but it does not involve cell creation. To our knowledge, type-B flow has not been observed in porous-media studies.

A further fluctuating state observed experimentally by Combarnous & Le Fur (1969) and Caltagirone, Cloupeau & Combarnous (1971) is similar to our case (ii). However, the numerical work of Horne & O'Sullivan (1974) shows that, unlike ours,

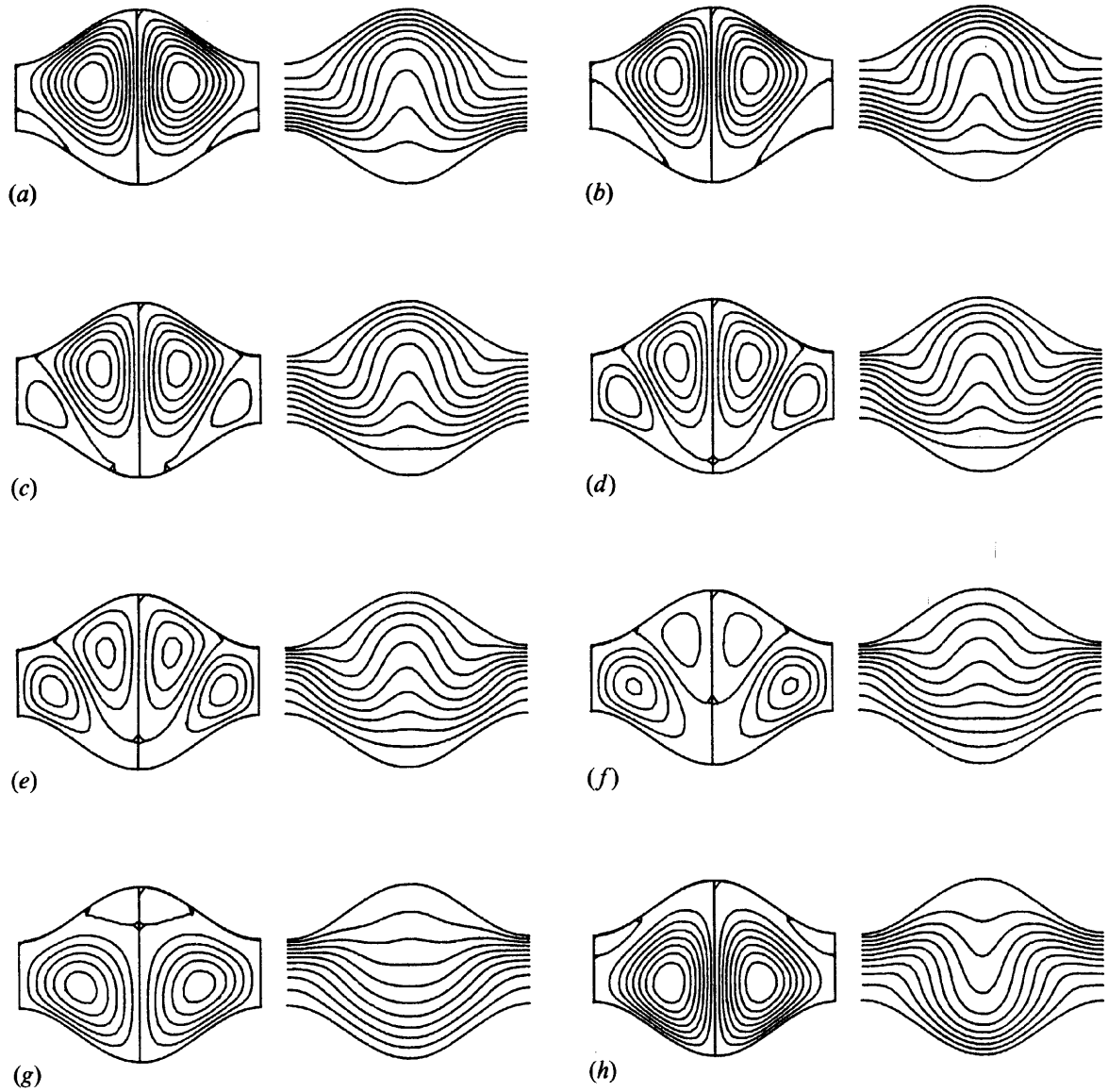

FIGURE 18. Instantaneous streamlines and isotherms for $Ra = 20$, $a = 0.45$, type II, for half a cycle. (*a*) corresponds to the maximum of $\psi_{\max}$, and consecutive plots are at equal time increments.

the flow is not periodic. The evolution of the streamlines and isotherms was not displayed in the numerical work, but may be found in Combarnous & Bories (1975) for the experimental work.

7. Conclusions

An analytical study of three-dimensional convection within an undulating porous layer heated from below has been presented. For $Ra \ll Ra_c$ the convection is weak and shares any symmetries of the geometrical configuration. For $Ra \sim Ra_c$, the flow bifurcates: when the layer is varicose, there is a supercritical bifurcation at a Rayleigh number which is dependent on the orientation of the resultant rolls, whilst for non-varicose configurations there is a smooth transition to a strongly convecting flow.

When the layer is varicose, there exists a purely transverse mode, the onset of which occurs when

$$Ra = Ra_c - 22.504a^2\delta^2 + O(\delta^4).$$

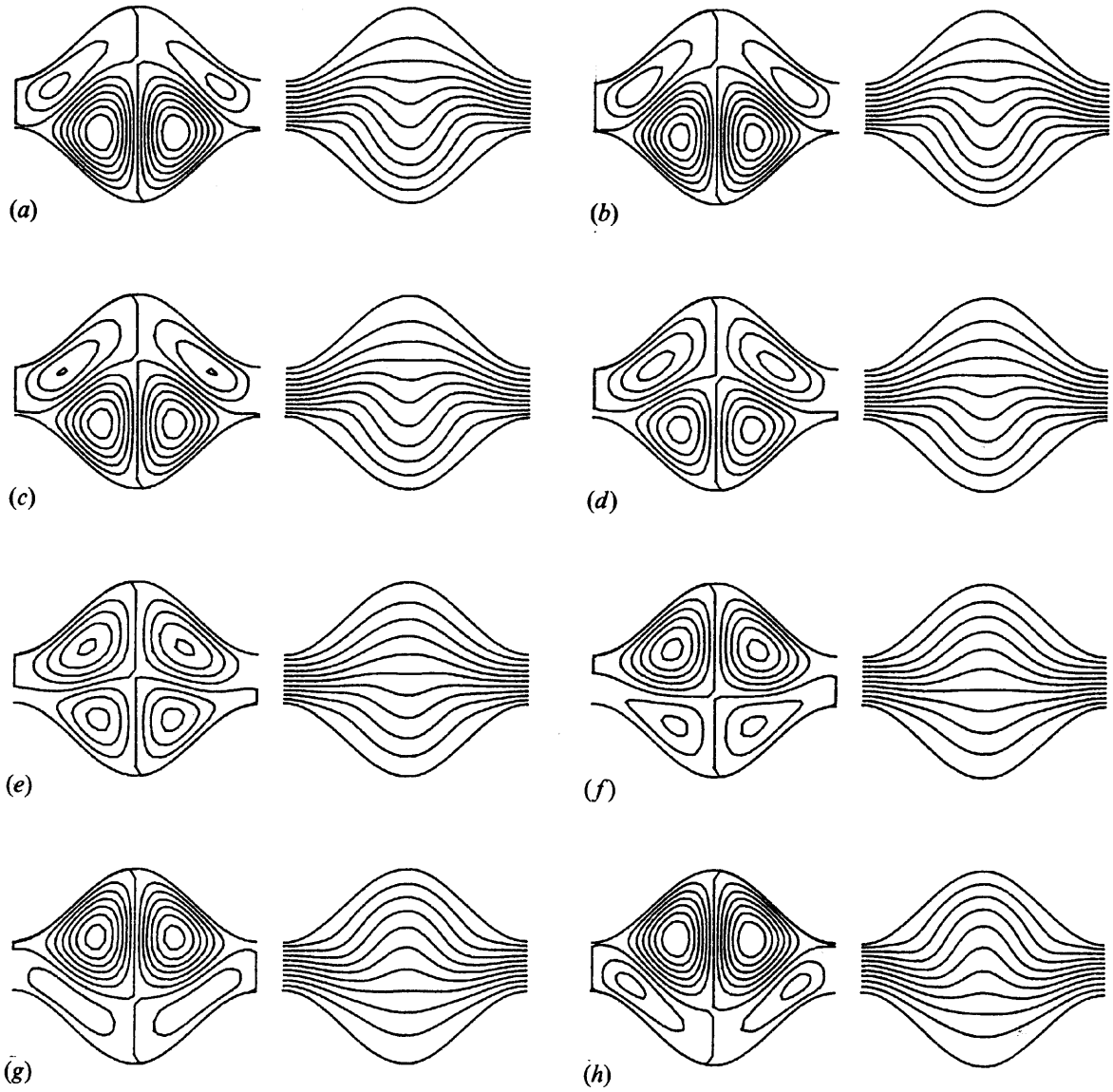

FIGURE 19. Instantaneous streamlines and isotherms for $Ra = 19$, $a = 0.6$, type II, for half a cycle. (a) corresponds to the maximum of $\psi_{\max}$, and consecutive plots are at equal time increments.

This Rayleigh number is less than those for the onset of types I and II longitudinal rolls, given by

$$Ra = Ra_c + 7.414a^2\delta^2 + O(\delta^4)$$

and

$$Ra = Ra_c + 9.380a^2\delta^2 + O(\delta^4)$$

respectively. It is expected, but we have not proved it, that the critical Rayleigh numbers for oblique rolls lie between the above values for transverse and longitudinal rolls. Thus stable transverse rolls appear at the first bifurcation. At a higher Rayleigh number (determined by (5.13)), stable longitudinal rolls may also exist. As regards the heat transfer, the mean Nusselt number for the supercritical regime is given by

$$\overline{Nu} = -1 + 4a^2\delta^2\overline{Nu}_V - \tfrac{1}{2}\epsilon^2 k_c^2(\hat{A}_L^2 + \hat{A}_L^2) + o(\epsilon^2, \delta^2),$$

where $\overline{Nu}_V \approx -0.214$ and $\hat{A}_L$, $\hat{A}_T$ are the amplitudes of the longitudinal and transverse rolls. It is clear from figure 8 that the transverse mode transports more heat than the longitudinal mode.

For non-varicose configurations, there is a smooth transition to strong convection

in the form of stable longitudinal rolls, and when the Rayleigh number exceeds $Ra_c + \delta^{\frac{2}{3}}[(357)^{\frac{1}{3}} k_c^2 c_p^2 - \frac{7}{3}\tilde{k}^2 Ra_c]$, there is also a stable mixed-mode solution. The mean Nusselt number is given by

$$\overline{Nu} = -1 - \tfrac{1}{2}\delta^{\frac{2}{3}} k_c^2 (\hat{A}_L^2 + \hat{A}_T^2) + o(\delta^{\frac{2}{3}});$$

the mode which maximizes the heat transfer is dependent upon the Rayleigh number and the amount of boundary detuning.

It should be noted that, although the results have been presented for boundary wavenumbers $\sim k_c$, the perturbation schemes may also be employed for more general wavenumbers. For example, when k is not a rational multiple of k_c, the double expansions of §5 may be used. The subharmonic and superharmonic cases generally require more subtle treatment (see Pal & Kelly 1978).

A numerical study of two-dimensional convection has also been presented for the varicose case only. Six types of flow have been highlighted. The first, for low Rayleigh numbers, consists of four cells per wavelength and corresponds to the steady quasi-conduction solution (3.16). The second and third are also steady flows and correspond to the types-I and -II solutions of §5.1 respectively. The final three are periodic and are typified by the cases (i), (ii) and (iii) presented in §6. Cases (i) and (ii) are examples of unsteady flows with the types-I and -II symmetries respectively. Case (iii) is an oscillatory form of quasi-conduction solution and has type-II symmetry. The boundary between the steady and unsteady flows has been determined in the parametric space of Rayleigh number Ra and boundary amplitude a.

Finally it is of interest to determine the thickness of a rock stratum so that the convective instability at $Ra_c = \pi^2$ may occur. For example, if we take a moderately permeable rock, such as sandstone, saturated with pure water, we have $K = 10^{-12}$ m^2, $\kappa = 10^{-8}$ m^2 s^{-1}, $\rho = 0.9923 \times 10^3$ kg m^{-3}, $\mu = 0.654 \times 10^{-3}$ kg m^{-1} s^{-1}, where the properties have been evaluated at 40 °C. Thus assuming a geothermal gradient of 0.025 °C m^{-1}, the stratum must be about 16 m thick for the onset of Lapwood convection.

The authors wish to express their gratitude to Professor Philip Drazin for many stimulating discussions on this problem and for comments on the draft of this paper, and to Dr Ian Walton for useful discussions on some aspects of the work. D.A.S.R. also wishes to acknowledge SERC support.

REFERENCES

Arakawa, A. 1966 Computational design of long-term numerical integration of the equations of fluid motion. I. Two-dimensional incompressible flow. *J. Comp. Phys.* **1**, 119–143.

Beck, J. L. 1972 Convection in a box of porous material saturated with fluid. *Phys. Fluids* **15**, 1377–1383.

Caltagirone, J. P. 1975 Thermoconvective instabilities in a horizontal porous layer. *J. Fluid Mech.* **72**, 269–287.

Caltagirone, J. P., Cloupeau, M. & Combarnous, M. A. 1971 Convection naturelle fluctuante dans une couche poreuse horizontale. *C. R. Acad. Sci. Paris* B **273**, 833–836.

Combarnous, M. A. & Bories, S. A. 1975 Hydrothermal convection in a saturated porous medium. *Adv. Hydr.* **10**, 231–307.

Combarnous, M. A. & Le Fur, B. 1969 Transfer de chaleur par convection naturelle dans une couche poreuse horizontale. *C. R. Acad. Sci. Paris* B **269**, 1009–1012.

Eagles, P. M. 1980 A Bénard convection problem with a perturbed lower wall. *Proc. R. Soc. Lond.* A **371**, 359–379.

ELDER, J. W. 1967 Steady free convection in a porous medium heated from below. *J. Fluid Mech.* **27**, 29–48.

FRICK, H. & MÜLLER, U. 1983 Oscillatory Hele-Shaw convection. *J. Fluid Mech.* **126**, 521–532.

HORNE, R. N. 1979 Three-dimensional natural convection in a confined porous medium heated from below. *J. Fluid Mech.* **92**, 751–766.

HORNE, R. N. & O'SULLIVAN, M. J. 1974 Oscillatory convection in a porous medium heated from below. *J. Fluid Mech.* **66**, 339–352.

HORNE, R. N. & O'SULLIVAN, M. J. 1978 Origin of oscillatory convection in a porous medium heated from below. *Phys. Fluids* **21**, 1260–1264.

KELLY, R. E. & PAL, D. 1976 Thermal convection between non-uniformly heated horizontal surfaces. In *Proc.* 1976 *Heat Transfer and Fluid Mech. Inst.* pp. 1–17. Stanford University Press.

KELLY, R. E. & PAL, D. 1978 Thermal convection with spatially periodic boundary conditions: resonant wavelength excitation. *J. Fluid Mech.* **86**, 433–456.

LAPWOOD, E. R. 1948 Convection of a fluid in a porous medium. *Proc. Camb. Phil. Soc.* **44**, 508–521.

PAL, D. & KELLY, R. E. 1978 Thermal convection with spatially periodic non-uniform heating: non-resonant wavelength excitation. In *Proc. 6th Intl Heat Trans. Conf. Toronto*, Vol. 2.

PAL, D. & KELLY, R. E. 1979 Three-dimensional thermal convection produced by two-dimensional thermal forcing. *ASME Paper* 79-HT-109.

PALM, E., WEBER, J. E. & KVERNVOLD, O. 1972 On steady convection in a porous medium. *J. Fluid Mech.* **54**, 153–161.

RIAHI, N. 1983 Nonlinear convection in a porous layer with finite conducting boundaries. *J. Fluid Mech.* **129**, 153–171.

ROACHE, P. J. 1972 *Computational Fluid Dynamics.* Hermosa.

SCHUBERT, G. & STRAUS, J. M. 1979 Three-dimensional and multicellular steady and unsteady convection in fluid-saturated porous media at high Rayleigh numbers. *J. Fluid Mech.* **94**, 25–48.

SCHUBERT, G. & STRAUS, J. M. 1982 Transitions in time-dependent thermal convection in fluid-saturated porous media. *J. Fluid Mech.* **121**, 301–313.

STRAUS, J. M. 1974 Large amplitude convection in porous media. *J. Fluid Mech.* **64**, 51–63.

TAVANTZIS, J., REISS, E. L. & MATKOWSKY, B. J. 1978 On the smooth transition to convection. *SIAM J. Appl. Maths* **34**, 322–337.

VOZOVOI, L. P. & NEPOMNYASCHII, A. A. 1974 Convection in a horizontal layer in the presence of spatial modulation of temperature at the boundaries. *Gidrodinamika* **8**, 105–117.

WALTON, I. C. 1982*a* The effects of slow spatial variations on Bénard convection. *Q. J. Mech. Appl. Maths* **35**, 33–48.

WALTON, I. C. 1982*b* On the onset of Rayleigh–Bénard convection in a fluid layer of slowly increasing depth. *Stud. Appl. Maths* **67**, 199–216.

WALTON, I. C. 1983 The onset of cellular convection in a shallow two-dimensional container of fluid heated non-uniformly from below. *J. Fluid Mech.* **131**, 455–470.

WATSON, A. & POOTS, G. 1971 The effect of sinusoidal protrusions on laminar free convection between vertical walls. *J. Fluid Mech.* **49**, 33–48.